Analytical Methods

ROYAL SOCIETY OF CHEMISTRY

CRITICAL REVIEW

View Article Online
View Journal | View Issue

Cite this: *Anal. Methods*, 2022, **14**, 4602

A review of electrochemical impedance spectroscopy for bioanalytical sensors

Edward P. Randviir * and Craig E. Banks

Electrochemical impedance spectroscopy (EIS) is a powerful technique for both quantitative and qualitative analysis. This review uses a systematic approach to examine how electrodes are tailored for use in EIS-based applications, describing the chemistries involved in sensor design, and discusses trends in the use of bio-based and non-bio-based electrodes. The review finds that immunosensors are the most prevalent sensor strategy that employs EIS as a quantification technique for target species. The review also finds that bio-based electrodes, though capable of detecting small molecules, are most applicable for the detection of complex molecules. Non-bio-based sensors are more often employed for simpler molecules and less often have applications for complex systems. We surmise that EIS has advanced in terms of electrode designs since our last review on the subject, although there are still inconsistencies in terms of equivalent circuit modelling for some sensor types. Removal of ambiguity from equivalent circuit models may help advance EIS as a choice detection method, allowing for lower limits of detection than traditional electrochemical methods such as voltammetry or amperometry.

Received 15th June 2022
Accepted 17th October 2022

DOI: 10.1039/d2ay00970f

rsc.li/methods

1. Introduction

Our previous review[1] took the reader on a whistle-stop tour of electrochemical impedance spectroscopy (EIS), from some basic fundamentals of EIS through to its applications, especially in the field of biosensors. The review took a brief look back at Oliver Heaviside's initial mathematical transformations and coining of the term "impedance", before examining a more contemporary understanding of diffusional impedance, reported by Warburg in the late 19th century. These principles preceded a closer look at how the technique was applied in several areas: from non-biological to biological systems, and from graphene composite materials through to screen printed electrodes (SPEs). We argued that the range of available target species and low detection limits made EIS into a promising prospect for it as a technique of choice within biological applications. Nearly a decade on, this update

Department of Natural Sciences, Faculty of Science and Engineering, Manchester Metropolitan University, Chester Street, Manchester M1 5GD, Lancs, UK. E-mail: E.Randviir@mmu.ac.uk; Tel: +44(0)1612471188

Edward Randviir is a Senior Lecturer in green and inorganic chemistry at Manchester Metropolitan University. His research encompasses fundamental and applied aspects of electrochemical impedance and electrochemical methods. He has been a consultant to the waste management industry and works on several waste-to-resource projects on materials ranging from textiles to road sweepings. He was also co-organiser for one of the world's first Twitter conferences, now an annual flagship event for the Royal Society of Chemistry known as #RSCPoster. He has over 30 published papers across several notable journals and has a h-index of 18.

Craig E. Banks holds a personal chair in nano- and electrochemical technology and has published over 550 papers (h-index: 91, Aug 22) and works on next generation screen-printed electrochemical sensing platforms as well the use of additive manufacturing in water splitting, sensor design, supercapacitors and battery development.

Table 1 Sub-categories of bio-based and non-bio-based electrodes

Bio-based	Non-bio-based
Oligonucleotide sensors	Molecularly imprinted polymer sensors
Aptasensors	Composite sensors[a]
Immunosensors	
Enzymatic sensors	

[a] Includes all other philosophies that are not MIPs.

review will examine whether EIS has emerged as a technique of choice within biological applications. It will investigate how researchers have continued to use the technique, especially focusing on whether and how implementation of the technique (in terms of electrode designs) has changed since our previous review.

The review will also examine some more recent fundamental understandings of EIS as a technique of choice. Only recently, a published paper by Randviir cross-examined the electron transfer rate constants (k^0) of EIS experiments when compared to voltammetric experiments, finding that there are potentially fundamental discrepancies between the two techniques when used in conjunction with printed carbon electrodes.[2] In order to make sense of this we will take the reader back to the works of Randles in the 1940s, examining the limitations and/or boundary conditions of EIS.

For the main body of this review, a systematic review process has been adopted. The search terms "EIS analytical" was combined with Boolean operators (NOT corrosion, environment, energy, battery, renewable, pollution) under a topic search on Web of Knowledge. This was intended to discount contributions intended for non-bioanalytical applications. After filtering the search results to show only original research articles, 481 results remained (as of March 2022). All results encompassing themes outside of the bioanalytical and EIS remit were excluded (*e.g.* corrosion, environmental, voltammetric or amperometric applications). The papers were further assessed for suitability by reading abstracts and filtering papers. For example, a significant number of papers use EIS as a *qualitative* technique to provide evidence of a successful electrode modification. Literature reports that have used EIS exclusively for reasons such as this have been discounted. This method returned 63 research papers that were grouped into "bio-based" and "non-bio-based" sensors to reflect the nature of electrode construction deriving from a biological or non-biological material. There were 48 bio-based and 14 non-bio-based works. The categories were further grouped into the sub-categories outlined in Table 1. Note it is possible that some key papers have been unintentionally discounted using this approach.

2. Electrochemical impedance spectroscopy (EIS)

The first part of this review focuses on the EIS experiment and some of the key fundamental mathematical derivations that underpin the modern EIS experiment. This serves as a "light" version of EIS and is not intended to be walking the reader through complex mathematics. It will, however, endeavour to summarize some of the key mathematical underpinnings of EIS and assess the concentration limitations of the modern EIS experiment. The information in this section brings together understanding of EIS from a range of sources.[1–6]

2.1 The EIS experiment

The EIS experimental setup connects a cell containing a target species (*e.g.*, the Fe^{2+}/Fe^{3+} redox couple) to a potentiostat using some number of electrodes depending upon the desired sensitivity. As is the case with voltammetric experiments, a three electrode system is often favoured that applies a potential between the working electrode (WE) and reference electrode (RE). Applying a potential between these electrodes disrupts the equilibrium of the cell and initiates the movement of electrons between the cell and the circuit, with the current generated measured between the working and the counter electrode (CE). The potential applied in an EIS experiment is frequency-dependent, in other words it is an alternating current (AC) potential applied across the electrodes as opposed to a DC potential in most electrochemical methods. This is often a small (10–20 mV) AC potential to create a pseudolinear relationship between current and voltage, which is a key experimental condition that allows EIS to be applied. In many experiments a DC potential is super-imposed upon this, which would normally correspond to a value close to the oxidation or reduction potential of the target analyte contained within the cell. The impedance, according to Ohm's law, can be determined as the ratio between the applied AC voltage at a given time, and the measured AC current arising as a result of the applied AC voltage. Since the technique applies AC signals and the measured current is not instantaneous (*i.e.*, there is a delay), the total impedance of the system is frequency-dependent. The basis of EIS is therefore to alternate the frequency of the experiment and measure the total impedance as a function of the frequency of the AC potential. In a typical modern EIS experiment, the software will perform this process repeatedly across a frequency range spanning 4–6 orders of magnitude; typically beginning at 100 000 Hz and scanning 10 frequencies per decade all the way down to 0.1 Hz. The data generated from this can be presented in a number of ways but two main methods are used: a Nyquist plot splits the total impedance into real and imaginary components and plots one against the other,† while a Bode plot shows the total impedance and phase angle as a function of the applied frequency.

Take for example the $Fe^{2+/3+}$ redox couple: a potentiostatic experiment will apply a step-changed voltage across the working and reference electrodes that will give rise to a current but only when the voltage reaches some thermodynamically favourable value (in the case of $Fe^{3+} \rightarrow Fe^{2+}$ this occurs at around −0.503 V‡ when using a saturated calomel electrode (SCE) as a reference). In this setup, the bulk concentration in the cell will comprise of only Fe^{3+} at $t = 0$ and a small equilibrium will form at the electrode surface prior to the experiment

† Impedance has real and imaginary components: resistance is frequency-independent and is considered the "real" component of impedance, while reactance is frequency-dependent and is considered the "imaginary" part of impedance. Reactance may be impedance due to capacitance or induction.

‡ Calculated from Fe^{3+} reduction potential of +0.771 V and Hg_2Cl_2 reduction potential of +0.2681 V.

commencing and will have its own voltage (known as the open circuit potential or OCP), which represents the electromotive force that is generated when the analyte is in contact with the electrical circuit (in the absence of an applied electric field). Voltammetric experiments force changes upon that equilibrium and, according to Le Chetalier's principle, this will encourage movement of electrons between the surface and the cell constituents, generating Fe^{2+} at the electrode surface to counteract the changes applied to the electrode. The movement of electrons generates the increased current on the voltammogram, which limits due to diffusion.

$$Fe^{3+} + e^- \rightarrow Fe^{2+} \quad (1)$$

EIS experiments differ significantly from this process because the common approach in EIS is not to force the equilibrium through potential sweeping between the RE and CE. Rather, the equilibrium is (normally) already established within the cell at the start of an EIS experiment by mixing equimolar concentrations of the oxidised and reduced species one would observe in the typical voltammetric counterpart experiment (so equal concentrations of Fe^{3+}/Fe^{2+}).§ To understand the reason for this experimental condition a simplified look back to original works by Randles is made.[4]

2.2 Equimolar concentrations

In Randles 1947 work, an argument was established that rapid electrode reactions, when subject to a small AC perturbation (in the order of around 7 mV) were electrically equivalent to a "capacity" and resistance in series. Randles wrote that when a cell is subject to AC fluctuations (eqn (2)), those fluctuations have a small effect on the chemical equilibrium in the cell (where V is the applied voltage perturbation, v is the effective voltage, ω is the angular frequency and t is the time).

$$v = V \cos \omega t \quad (2)$$

Displacement of the chemical equilibrium results from this voltage, since the perturbation is a few mV from the equilibrium potential, so it follows that even a brief move away from this potential will cause momentary imbalance in the chemical equilibrium, generating a current signal due to the movement of electrons. The current generated then is proportional to the point on the wave period at time t. Production of this current is not always immediate, however. Rather there is a time delay between application of the AC voltage and the production of current, resulting in an AC current out of phase with the applied voltage. This is termed as the shift in phase angle and is given the notation θ (eqn (3)).

$$i = I \cos(\omega t + \theta) \quad (3)$$

Returning to Randles, these momentary displacements in equilibrium are, in effect, changes in concentration of two species: when one species is oxidised (*e.g.*, Fe^{2+}), the other species is being reduced (*e.g.*, Fe^{3+}) and *vice versa* when the AC period progresses to the opposite bias. These small concentrations are assumed to dissipate within the bulk solution. The observed concentration variation (ΔC) is then also proportional to the point in time along the wave period according to eqn (4), where δC is the calculus function for concentration.

$$\delta C = \Delta C \cos(\omega t + \theta) \quad (4)$$

Solving Fick's second law for linear diffusion using eqn (4) as a boundary condition is the fundamental basis for Randles' idea that rapid electrode reactions can be modelled using capacity and resistance in series. The basis of modern EIS is therefore underpinned by the idea that the concentrations of the two species must be equal at the beginning of the experiment, for if they were not equal, there would be a non-equilibrium state at the electrode surface, whereby a concentration gradient would form, giving rise to a voltage larger than the AC perturbation. The phenomenon described above, where small concentration fluctuations occur marginally either side of the equilibrium potential would not be observed. Noteworthy is that Randles solves Fick's second law using this boundary condition under the assumption of a linear diffusion model, though the experimental work uses microelectrodes that exhibit hemispherical diffusion, so perhaps this is a limitation to the original work reported by Randles.

In a practical sense, setting the cell with equimolar concentrations of the oxidised and reduced species is required. This may be achieved either through mixtures of equimolar concentrations of oxidised and reduced species from the very beginning, or alternatively beginning with only one species in the cell and superimposing a DC potential upon the AC perturbation such that equal concentrations of products and reactants are achieved (*i.e.*, applying the half-wave potential, $E_{1/2}$). Randles disputed the idea that superimposing a DC potential at $E_{1/2}$ was in effect the same as starting with equimolar species in the cell. As was put, applying the DC potential to achieve equimolar concentrations of target species is, in effect, "a steady state of the diffusion layer", which is not applicable to the alternating current process. Randles was assuming that the AC variation occurred at the electrode surface only and not across the diffusion layer. This may also suggest that the smaller the diffusion layer, the more accurate the experiment when superimposing a DC potential. Despite the criticism, Breyer and Gutmann's theoretical paper, and subsequent experimental confirmation describing DC-superimposed experiments, showed that applying the superimposition on a reversibly depolarised electrode resulted in current maxima around the standard potential of the system;[5] some researchers still use the DC superimposition method today.

2.3 EIS basic data analysis

EIS is a powerful tool for obtaining information on the nature of electrode processes. While studying literature reports on EIS, researchers will almost always discover that authors report EIS spectra with accompanying equivalent circuit models, which are essential for the fundamental understanding of the exact

§ Alternatively, a DC potential can be simultaneously applied to the circuit.

nature of the electrode process, and for yielding of meaningful quantitative data from an EIS experiment. Unfortunately, equivalent circuit models are sometimes constructed without a theoretical basis and instead constructed to match the data observed without consideration of the exact nature of the electrode process. Yet, it is from construction of the equivalent circuit models, and subsequent data fitting, that accurate quantitative values for several parameters can be extracted. Some common electrode designs with corresponding (indicative) Nyquist plots and equivalent circuit models are presented in Fig. 1.

From the equivalent circuit models in Fig. 1 it is seen that numerous elements can be quantified using data processing software, which can then be related to the physical processes occurring. Most commonly the charge transfer resistance, R_{CT}, is used to describe how effective the electrode is at oxidising or reducing a species, which can then be related to a specifically designed event at the surface. Fig. 1A depicts an unmodified working electrode (*e.g.*, a gold electrode) immersed within a Fe^{2+} bulk solution. During the EIS experiment, some DC potential (*e.g.*, the open circuit potential for $Fe^{2+/3+}$) is applied between the working and reference electrodes, forming a diffusion layer at the electrode surface. The Nyquist plot

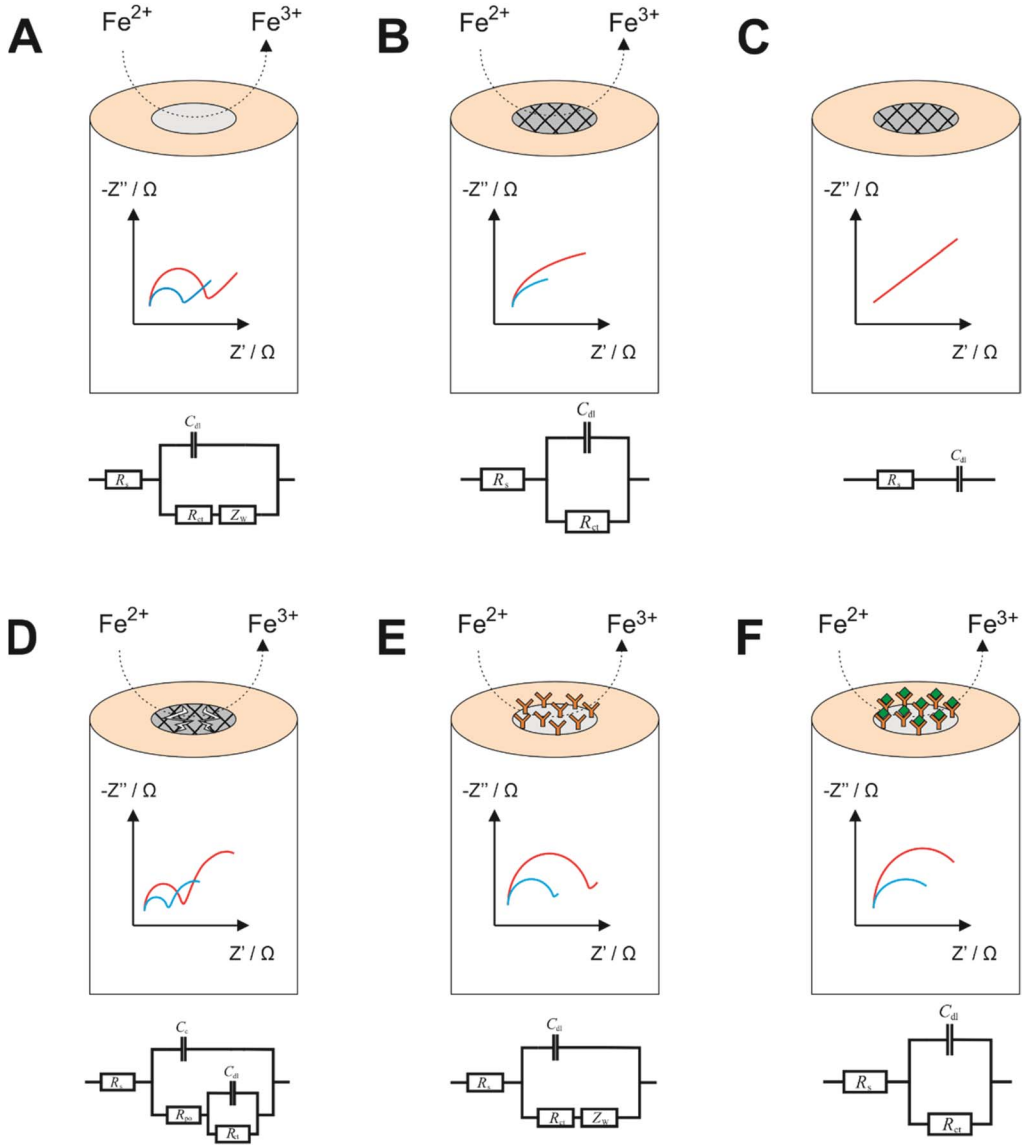

Fig. 1 A non-exhaustive graphical description of electrode surfaces with complimentary Nyquist plots from an EIS experiment, and an equivalent circuit model that may match the experimentally observed EIS profile. (A) An unmodified macroelectrode in the presence of a redox couple; (B) an electrode coated with an insulating layer in the presence of a redox couple; (C) an electrode with an insulating layer without the presence of a redox couple; (D) a failed coating in the presence of a redox couple; (E) an electrode modified with an antibody in the presence of a redox couple; (F) an electrode modified with an antibody bound to its complimentary antigen in the presence of a redox probe. The blue lines indicate the same experiment with a higher concentration of redox probe, since impedance is inversely proportional to the concentration of the bulk species.

obtained from this experiment may look similar to the one observed in Fig. 1A, whereby the semicircle begins at some value of Z' greater than 0 (this is the solution resistance, R_S). The width of the semicircle is the R_{CT}, while the straight line at a 45° angle is indicative of impedance due to diffusion. Fig. 1B is an indicative EIS profile of an electrode with an insulating coating in the presence of a redox couple. In this instance the EIS profile will not witness a complete semicircle because the frequency domains of effective charge transfer and diffusion overlap. The R_{CT} is very high due to the insulating nature of the coating, which leads to charging of the coating surface at low frequencies and therefore increased impedance. The same case is presented in Fig. 1C, but in the presence of a cell without a redox couple. In this case, the EIS profile has lost its R_{CT} component because the redox couple isn't present to transfer charge. Effectively the only phenomenon occurring is charging of the insulating layer from the electrolyte, reflected in the circuit model and the profile. Also of note is that because there is no redox couple, concentration is not a factor as in all other cases (hence only 1 line on the spectrum). Fig. 1D shows an impedance profile with two time constants, indicative of a failed coating. In the higher frequency domain, there is a R_{CT} observed as a result of the oxidation of Fe^{2+} to Fe^{3+} like in Fig. 1A, while in the low frequency domain there is a second process which is more akin to that observed in Fig. 1B, so in effect a combination of two processes observed in one profile. This is modelled by replacing the diffusional term in Fig. 1A with another capacitor and resistor in parallel. R_{PO} is described as the pore resistance, while C_C is the charge resulting from occupation of such pores by charged species. Fig. 1E and F show how a biorecognition event might be modelled using a redox couple. In Fig. 1E, and antibody grafted upon an electrode may permit a small amount of redox couple to and from the electrode surface, hence potentially could be modelled using the diffusional Randles model depicted in the circuit model below the impedance profile. Upon antibody/antigen binding, more material at the electrode surface may permit less of the redox couple to the surface or a slower rate of diffusion to and from the electrode may be observed. The only redox couple at the surface may remain trapped, unable to diffuse away. This model could remove the diffusional impedance term. In all cases except Fig. 1C, the blue line represents the higher concentration of redox probe, since the R_{CT} is inversely proportional to the concentration according to eqn (5), assuming equimolar concentrations of the oxidised and reduced species, where R is the molar gas constant, T is the absolute temperature, n is the number of electrons transferred, F is the Faraday constant, k^0 is the electron transfer rate constant and C is the concentration of the bulk species.

$$R_{CT} = RT/n^2F^2k^0C \quad (5)$$

Noteworthy is the ambiguity of equivalent circuit modelling. As alluded to previously many equivalent circuit models appear to be constructed without a theoretical basis, potentially rendering any subsequent data analysis potentially inaccurate or obsolete.[6] One example of that is in the work by Hashem and co-workers who provide quite a complex circuit model for the molecularly imprinted polymer sensor without philosophical basis for each component.[7] Then there are cases where attempts are made at explaining equivalent circuit models, which in themselves are quite erroneous, such as including reference electrode contributions to impedance within a three electrode system despite current not being measured at the reference electrode![8] Perhaps a valuable future contribution to the field might be a reference tool for equivalent circuit modelling, which could clear up some ambiguity for users.

Returning to eqn (5), this expression has itself been used analytically and qualitatively by the author in previous work, which showed that EIS can be used not only to determine concentrations of *quasi*-reversible redox systems with a high degree of accuracy, but potentially even electrochemical rate constants for irreversible systems, something that is not achievable using Nicholson or Laviron methods.[2]

3. Applied electrochemical impedance spectroscopy

The remainder of this review will examine literature reports that have utilised EIS as the analytical detection method. While many literature reports utilised EIS within their work, the technique appears to be more frequently employed in a qualitative sense. That is, when researchers design electrode materials, EIS is used at each step of the electrode construction process to confirm successful immobilisation of electrode modifications. Literature reports that use EIS *only* in this way have been discounted from this section (there are several examples of this that were filtered from this review from 2021 and 2020[7,9–27]). Instead, this section seeks to present literature reports of EIS when used as the technique of choice for generating a *quantitative* analytical signal. This section is split into the two categories: bio-based; and non-bio-based sensors. Within both categories there are sub-categories that will be discussed, and more detail is provided for the more interesting applications of the technique, in terms of electrode construction and obtained spectra.

3.1 Bio-based sensors

This section focuses exclusively on the bio-based sensors identified from the literature since 2013. When referring to a sensor as "bio-based", that is defined in this section as an electrode sensor that has been, either fully or (normally) partly, constructed from a natural (or synthetic natural) material. This might be an electrode designed using proteins, oligomers or antibodies. Using this definition, the application of the sensor itself may not be "biological" itself, but in most cases it is. There are four types of bio-based sensors witnessed within the scientific literature: (1) immunosensors; (2) aptamer sensors; (3) oligonucleotide sensors; and (4) enzymatic sensors. Phage-display sensing strategies are also researched but none were captured within the systematic review.[101] Immunosensors have by far been the most closely studied sub-category within this sample of literature, accounting for 34 of the 51 papers

discussing EIS as a quantitative immunosensing technique. Aptasensors account for 9 papers, while oligonucleotide and enzymatic sensors account for 5 and 2 research papers, respectively. The is one extra paper that uses proteins as a detection element, that has been discussed in the enzymatic sensor section.

3.1.1 Immunosensors. Immunosensing is the process whereby an antibody/antigen binding event occurs that leads to the production of an analytical signal. The analytical signal might be the production of light of a specific wavelength for spectroscopic sensors, but for the purposes of EIS the signal generated is a change in measured impedance (*i.e.*, a change to the current signal produced of a redox system under the influence of a fixed AC voltage) as a result of the antibody/antigen binding event. In EIS immunosensor experiments, an antibody is normally grafted onto the working electrode, using a range of crosslinking chemicals, polymers, nanoparticles or self-assembled monolayers, such that the electrolyte-facing part of the electrode is the antibody. Running an EIS experiment using the antibody electrode immersed within a cell containing a redox couple in the bulk solution provides a value for charge transfer resistance (R_{CT}), which can be visualised graphically as the diameter of a semicircle in a Nyquist plot. In principle, if the antibody modified electrode is incubated in a medium containing a complimentary antigen, the bound antibody/antigen complex will alter the electrochemical signal because there is more material influencing passage of the redox probe to the electrode surface; the R_{CT} value (or semicircle diameter) should increase if the added material is more resistive. For analytical detection, if this increase in R_{CT} is proportional to the concentration of the antigen within the incubation medium, then EIS can be used analytically. EIS is a useful tool to detect a whole range of antigens ranging from human papillomavirus (HPV) through to Covid-19.

The difficulty with immunosensors is to be able to design an electrode that is conductive enough to be able to produce an electrochemical signal for a target redox probe, while at the same time providing a stable foundation for the antigen to bind to, and not be displaced easily, while also remaining upright such that the binding event can occur (*i.e.*, so binding sites are not hindered). Then the electrode must also be able to specifically target the antigen without interference from common interferents (*e.g.*, simple molecules such as ascorbic acid or uric acid) and have a good level of stability such that the electrode can be stored and/or reused. This leads to a range of different electrode designs, most incorporating in excess of 4 different components to the electrode. Table 2 lists several examples of the applications of EIS using immunosensing as the detection philosophy – some of the more promising candidates are discussed herein.

It is clear from Table 2 that there is a vast range of electrode substrates and modifications that make up the immunosensors in the literature. Beginning with Ben Halima and co-workers, a silicon nitride (Si_3N_4) electrode substrate is used to build the immunosensor for the quantification of tumour necrosis factor-α (TNF-α), which is one of several biomarkers for heart failure.[28] The approach links anti-TNF-α to the electrode substrate, first by activating the Si_3N_4 substrate under UV and O_3 to form hydroxyl groups on the surface.¶ The activated electrode is then subjected to triethoxysilyl undecanal (TESUD) in the vapour phase to provide a bridge between the electrode substrate and the sensing element (*i.e.* anti-TNF-α). TESUD is one of many different types of silyl cross linkers (depicted in Fig. 2 alongside some others) that are commonly used to covalently attach sensing elements to electrode substrates in electrochemical sensor designs. Once TESUD is attached, the aldehyde functionality spontaneously forms covalent bonds with anti-TNF-α. This is achieved by immersing the electrode in a known concentration of the antigen in solution. Most immunosensor electrodes are then subjected to a final step, which is immersion in a substance that blocks non-specific binding sites. In the work by Halima and co-workers, ethanolamine performs this function,[28] however other substances are also commonly used, such as bovine serum albumin (BSA) and glycine. A novel aspect of this approach is that the immunosensor displays functionality within non-invasive media. As is witnessed in Table 2, most researchers favour serum samples as the real medium to test their sensing platforms. Yet a saliva-based sensor would circumvent the need for invasive procedures, *e.g.*, blood sampling. A saliva-based sensor is also the focus of work by Aydın and co-workers.[29] Interleukin 8 (IL-8) is the focus of their work, whereby an ITO electrode is coated with polymers and conductive carbon black (perhaps to overcome resistivity of the polymer layer and to ensure oxidation of the redox couple) to house the anti-IL8 biorecognition element. A good analytical performance is observed for the sensor, coupled with an impressive recovery rate of IL-8 from saliva (99–101%) using ELISA as a benchmark technique. The sensor displays 90% performance after 5 weeks storage.

Immunosensors are also constructed using paper-based substrates. Work by Li *et al.* demonstrates that using paper substrates, target antibodies can be attached to carbon ink and zinc oxide nanowires (ZnO NWs) using cross linkers.[30] The paper-based substrate, cellulose paper, is printed with wax to simultaneously provide hydrophobicity and electrode shape definition. Like screen printing, carbon layers are printed into counter electrode directly onto the paper substrate. The working electrode is formed by hydrothermal growth of ZnO NWs directly onto the paper/carbon substrate. The working electrode diameter is clamped between glass slides, exposing the working electrode to air. Several aliquots of ZnO nanoparticle suspensions are drop-casted and dried onto the substrate to seed the electrode. When seeding is complete, the clamped electrode is suspended into a vial of ZnO NPs and heated to 86 °C for 8 hours to allow the nanowires to form. The nanoparticle formulations are changed according to the desired length and thickness of the NWs, before attachment of the

¶ Forming OH groups on electrode surfaces is commonplace in the design of many electrochemical sensors. Hydroxyl groups are essential for the formation of covalent bonds between the electrode and parts of the sensor. Throughout this review we will draw attention to several examples using a range of approaches to achieve this.

Table 2 A table of selected examples of immunosensors that employ EIS as the recognition technique

Year	Medium	Electrode	Target	Remarks	Ref.
2022	Human serum	GCE, GCN-β-CD,[dd] AuNPs, anti-25(OH)D_3	25(OHD_3)[ee]	Combined DPV and EIS sensor but EIS shows lower limit of detection	61
2021	Blood	SPE, AuNP, DHP,[ff] anti-DD	D-dimer	Diffusionless impedance profile	62
2021	Saliva	Si_3N_4-TESUD-anti-TNF-α[a]	Tumor necrosis factor-α	Unaffected by matrix effects	28
2021	Human serum	Paper, ZnO nanowires	HIV, Covid-19	Versatile method for sensor development	30
2021	Human serum	Au-SPE, cysteamine, Ab-CEA	Carcinoembryonic antigen	*In situ* EIS and SERS method useful for EIS validation at point-of-care	31
2020	Aqueous	Au-SPE, 4-ATP[b], GLA[c], anti-RSV	Respiratory syncytial virus	Specificity is observed but not tested in real media	63
2020	Human serum	Ni-foam, NH_2-MIL-88B(Fe_2Co)[d], anti-cTnI	Cardiac troponin I	Authors make arguments based on low LOD, but in practice the low LOD isn't necessary due to the diagnostic range of troponin required	64
2020	Cell cultures	ITO[e], APTES,[f] EDC/NHS,[g] anti-Tf	Transferrin	Limited dataset	65
2020	Human serum	ITO, PET, 3-GOPS,[h] anti-SOX_2	SOX_2	Diffuse voltammetric signals towards $[Fe(CN_6)]^{3-/4-}$ may be a reason for selecting EIS	32
2020	Human serum	Au, PEA, SA,[i] anti-P53	P53	~90% recovery in serum spike experiments	33
2020	Human serum	SPE, AuNP, Au-nano dendroids, GO,[j] anti-ALP	Alkaline phosphatase	Unusual Nyquist plots revealing possibly two time constants	66
2019	Human serum	ITO, PET, GPTES,[k] anti-TNF	Tumour necrosis factor-α	Limited real sample analysis	34
2019	Human serum	ITO, PET, 3-CPTMS,[l] anti-PAK2	PAK2	Good reproducibility in artificial and real samples	67
2019	Cerebrospinal fluid	ITO, AuNP, poly(glutamic acid), anti-α-SYN	α-Synuclein	4–2000 pg mL^{-1} detection range	68
2019	Human serum	GCE, AuNP, rGO,[m] anti-PSA	Prostate specific antigen	Poor analytical sensitivity	69
2019	Saliva	Au-paper, BSA, Ab-E[n]	H1N1	Dual colorimetric and impedimetric approach allows for rapid visual detection coupled with quantitative analysis	70
2018	Human serum	ITO, chitosan, CB,[o] GLA, anti-P53	P53	25% reduction in activity after 3 weeks storage	35
2018	Human serum and saliva	ITO, PET, SPGMA, CB, PVDF,[p] anti-IL-8	Interleukin 8	99–101% recovery shown for IL8 from diluted real samples – ELISA used to benchmark	29
2018	Human serum	ITO, CPTMS, anti-CRP	C-reactive protein	Linear range is so low that it would not necessarily detect patients with high levels of the protein	71
2018	Human serum	SPE, GQD, AuNR,[q] anti-PSA	Prostate specific antigen	Sensor can also be modified as an aptamer, which shows improved storage capability	42
2017	Human serum	Au, cysteamine, PDITC, CFTR/DYS[r]	Cystic fibrosis transmembrane regulator/Duchenne muscular dystrophy	Method validated with ELISA. Linear range established over 6 orders of magnitude	72
2017	Human serum	ITO, 3-GOPS, anti-MAGE1	Melanoma antigen	Voltammetric and impedimetric approaches both possible	73

Table 2 (*Contd.*)

Year	Medium	Electrode	Target	Remarks	Ref.
2017	Human serum	ITO, 3-GOPS, anti-MAGE-1	Melanoma antigen	Impedimetric data more promising than voltammetric and good shelf life observed	74
2016	Human serum	GCE, GO, EDC/NHS, anti-HSP70	Heat shock protein 70	Detection ranges several orders of magnitude narrower than commercial ELISA methods	75
2016	Aqueous solutions (IgG) and human serum (HIV)	Paper, ZnO nanowires, APTMS, GA, anti-rabbit IgG OR P24 antibody	Rabbit IgG or HIV	Nyquist plots shows a very wide but flat profile, potentially inferring that the device shows increased charge storage	76
2016	Human serum	Au, MHA[s], EG_3SH[t], amine-PEG3-biotin[u], avidin, ^{Btn}Ab-Ag_{PSA}-^{HRP}Ab	Prostate specific antigen	Two time constants on the Nyquist plots	37
2016	Human serum	SPE, nitrocellulose membrane, anti-BSA	Bovine serum albumin	Uses a smart phone detection system – promising but dataset seems thin	77
2015	Human serum	GCE, GO, chitosan, thionine, anti-PSA AuNP, PAMA[v], GA, HRP, streptavidin, biotin	Prostate specific antigen	Combined immuno- and aptasensor – applied to prostate cancer cells	39
2015	Human serum	Au, MUA[w], C6OH[x], anti-NS1	Non-structural dengue protein	C_6OH used as a spacer	78
2015	Human serum	GCE, MWCNT[y], GO[z], PyBuNHS[aa], anti-cTnI	Human cardiac troponin-I	0.94 pg mL^{-1} detection limit – use of a low n value constant phase element could potentially affect reliability	79
2015	Aqueous	SPE, dynabeads,[bb] anti-human IgG	Human IgG	Detection philosophy uses hydrogen evolution instead of the typical $Fe^{2+/3+}$ couple	80
2014	Hen serum	GCE, proteinA, anti-HisA	H5N1 influenza virus	Direct grafting of antibody onto the electrode *via* generation of carboxylic acid groups on GCE	81
2014	Urine	Au-SPE, cysteamine, anti-8OHdG	8OHdG[cc]	Slightly better linearity for EIS than for DPV	82
2014	Human serum	Au-SPE, cysteamine, anti-oxLDL	Lipoprotein	Sensor is formed using three monoclonal antibodies	83

[a] Triethoxysilyl undecanal. [b] 4-Aminophenol. [c] Glutaraldehyde. [d] Metal organic framework hydrothermally synthesized onto the Ni foam from Fe_2Co, 2-aminoterephthalic acid, dimethylformamide and acetic acid. [e] Indium tin oxide. Electrodes are activated using a 1 : 1 : 5 solution of $NH_4OH : H_2O_2$: water. [f] (3-Aminopropyl)triethoxysilane. [g] *N*-(3-Dimethylaminopropyl)-*N*′-ethylcarbodimide hydrochloride/*N*-hydroxysuccinimide. [h] Polyethylene terephthalate, 3-glycioxypropyl trimethoxysilane. [i] Succinic acid. [j] Gold nanoparticles, graphene oxide. [k] (3-Glycidyloxypropyl) triethoxysilane. [l] (3-Chloropropyl)trimethoxysilane. [m] Reduced graphene oxide. [n] Bovine serum albumin, anti-influenza antibody. [o] Carbon black. [p] SPGMA is ambiguously termed as "star polymer", polyvinyldenefluoride. [q] Graphene quantum dots, gold nanorods. [r] Phenylene diisothiocyanate. [s] 16-Mercaptohexadecanoic acid. [t] Tri(ethyleneglycol)thiol. [u] (+)-Biotinyl-3,6,9-trioxaundecanediamine. [v] Polyamido amine dendrimers. [w] 11-Mercaptoundecanoic acid. [x] 6-Mercaptohexanol. [y] Multi-walled carbon nanotubes. [z] Graphene oxide. [aa] 1-Pyrenebutyric acid *N*-hydroxysuccinimide. [bb] Dynabeads M-280. [cc] 8-Hydroxy-2′-deoxyguanosine. [dd] Graphitic carbon nitride and β-cyclodextrin. [ee] Serum 25-hydroxyvitamin D. [ff] Dehexadecyl phosphate.

sensing probe. In their work, several sensing probes are used, the most notable being the SARS-CoV-2 spike protein receptor binding domain. The spike protein is covalently bonded to the ZnO NWs through the use of APTMS and glutaraldehyde (GA).‖ Fig. 3 shows how the R_{CT} of the electrode increases as the concentration of recombinant IgG antibody (CR3022) to SARS-CoV-2 spike glycoprotein S1 increases within human serum samples. Concentrations of up to 1 μg mL^{-1} of recombinant antibody can be detected using the paper-based approach, representing a low cost disposable sensor strategy for Covid-19 and many other infectious diseases. In particular the authors argue that this approach can compliment mass polymerase chain reaction (PCR) testing by determining asymptomatic

‖ Another common cross-linker used for biosensors.

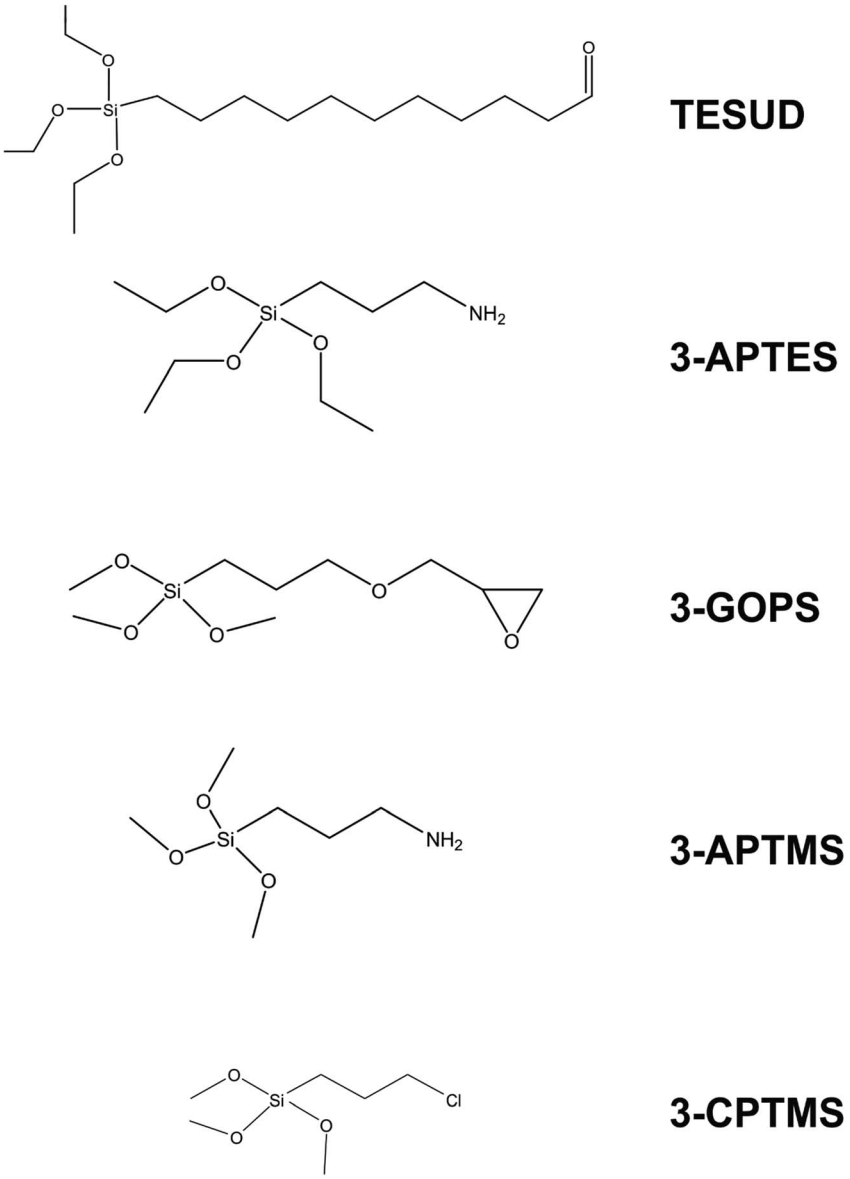

Fig. 2 Common silyl-based cross linkers employed for effective linkage of biological species to electrodes.

infection.[30] A potential drawback of this approach is the need for human serum, when a non-invasive fluid, *e.g.* saliva or nasal swab, would be more preferable for the patient.

Dual detection approaches are also witnessed for immunosensing, with work by Castaño-Guerrero focusing on surfaced enhanced Raman spectroscopy (SERS) combined with EIS for the observation of cancer biomarkers.[31] Their work focuses on carcinoembryonic antigen (CEA), which is a cancer biomarker employed in a clinical context that is mostly associated with colon and gastric cancers. The electrode design employs a gold screen printed electrode (Au-SPE) that is cleaned and drop-casted with 100 mM cysteamine, which self-assembles onto the surface *via* gold–sulfur chemistry, leaving the amine functionality exposed. Meanwhile, the CEA antibody (Ab-CEA) is activated using a combination of *N*-hydroxysuccinimide (NHS) and *N*-(3-dimethylaminopropyl)-*N*′-ethyl-carbodiimide hydrochloride (EDC), which is another common approach observed within the literature for the covalent attachment of antibodies to electrodes (Fig. 4). EDC activates carboxylic acid groups, that spontaneously form covalent bonds with amines; in this case, cysteamine. NHS is used as a protecting group for the reactive intermediate formed from EDC activation, but it allows spontaneous coupling to primary amines at physiological pH, which is a process exploited in many electrode designs. Glycine is used as a blocking agent to prevent electrochemical signals arising from non-specific binding sites. After CEA is hybridised to the electrode, the EIS signal is generated using a $Fe^{2+/3+}$ redox probe. After EIS measurement the SERS probe is attached, which consisted of gold nanostars (Au-NS) functionalised with 4-aminothiophenol (4-ATP) then crosslinked to activated Ab-CEA. The AuNS/4-ATP/AbCEA is then added to the EIS sensor probe for SERS measurement after EIS readings are taken. Under conditions of

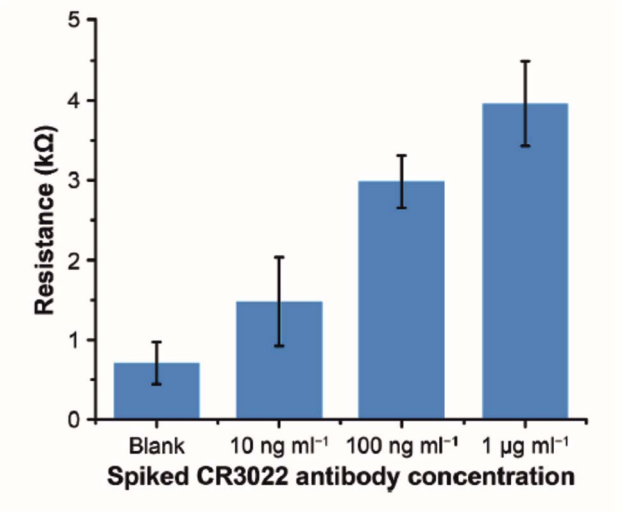

Fig. 3 Experimental results of detecting CR3022 antibody (specific to SARS-CoV-2 spike glycoprotein S1) in human serum. Error bars represent standard deviations ($n = 5$). Reprinted from ref. 30 with permission from Elsevier *via* Rightslink.

pH 4.5, a linear correlation between R_{CT} and CEA concentration is observed for the sensor between CEA concentrations of 0.25–250 ng mL^{-1}.[31] Similarly, the electrode is employed in serum samples, yielding a similar correlation within the same range, although sensitivity was slightly perturbed due to matrix effects. There is also a slight change in sensor performance when in the presence of common interferents found in serum (*e.g.* creatinine and glucose). The SERS procedure is able to detect 10× lesser concentrations than EIS, to a slightly lesser sensitivity. The authors argue this is not an issue for the EIS sensor because the LoD for the EIS sensor is well within the CEA range for a healthy patient. Hence, the work provides a potential *in situ* validation method for EIS analytical testing within a clinical setting.

Examples to this point have focused on human serum as a medium but other media are also explored for immunosensing. The focus of work by de Almeida *et al.* is to discriminate between cancerous and non-cancerous cells using EIS. Their work employs an indium tin oxide (ITO) electrode functionalised with APTES, EDC/NHS and finally anti-Tf (transferrin). The detection philosophy takes advantage of cancer cells over-expressing the Tf antibody, which is exploited in this work by immersing the activated ITO/APTES electrode in cancerous or non-cancerous cells. In this case, covalent bonds form between the carboxyl groups activated by EDC/NHS chemistry and anti-Tf, which transfers from the cell surface to the electrode. Therefore, the cell itself acts as the immunosensor because, if cancerous, it will over-express the Tf antibody at the electrode surface. If the antibody is at the surface, a biorecognition event between anti-Tf and Tf can occur. If uncancerous, the anti-Tf will not be expressed to the same degree and this will theoretically reduce the R_{CT} observed upon hybridisation with Tf. A change in R_{CT} observed towards $[Fe(CN)_6]^{3-/4-}$ is observed both for healthy any cancerous cells, however the changes are more significant for cancerous cells. The work shows a promising method for detection of cancerous cells rather than from other media, however further work on exploring a larger concentration range, using a larger range of cancerous cells would be required to consolidate this detection philosophy into something more translatable to clinical practice.

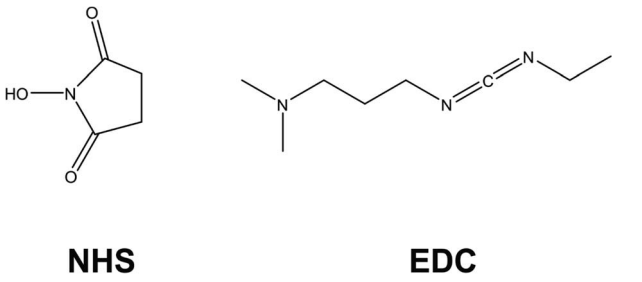

Fig. 4 Chemical structures of *N*-hydroxysuccinimide (NHS) and *N*-(3-dimethylaminopropyl)-*N*′-ethyl-carbodiimide hydrochloride (EDC), which are regularly used in combination to functionalise oxygenated terminal species on surfaces.

Many research papers utilise voltammetry for immunosensors. However, there are several other cases where voltammetric profiles observed for immunosensors are diffuse,** and in these cases the reliability and reproducibility of the voltammetric signal may be compromised. EIS might be the favoured technique in such examples. Immunosensor reports with diffuse voltammetric waves are provided for interest.[32–34] One example is that of Adeniyi and Mashazi, who report the impedimetric detection of cancer formation. Their work uses voltammetric cycling to bond phenylethylamine (PEA) to a gold electrode. Then, succinic anhydride is self-assembled onto the PEA and activated using EDC/NHS chemistry. Anti-P53 was self-assembled onto the electrode therein. Their data shows promise but with a caveat of low recovery in spiked serum experiments. Similarly, Aydın *et al.* report their immunosensor targeting P53,[35] which is based on an ITO electrode functionalised with chitosan and carbon black, the former being a common material for electrode layer formation in electrochemical diagnostics due to its biocompatibility. The electrode is modified with anti-P53 by cross-linkage with GA. The sensor shows some promising analytical capability for low concentrations of P52 in the pg range but suffers from poor regeneration capability and 25% loss in sensor activity after 3 weeks of storage.

In summary this section on immunosensors finds them to be the most prevalently researched application of EIS as an analytical detection method for bioanalysis, and this is achieved using a range of sensor design strategies. Sensors are frequently reliant on the existence of –OH terminating species on the underlying electrode substrate, upon which the electrode is constructed upon. Cross-linking chemistries are used to covalently attach antibodies to the electrode surfaces, making modern design strategies appear far more stable than

** Diffuse voltammetric profiles are those that experience increased peak-to-peak separation relative to the underlying electrode material, as well as a compromised peak current. These two factors suggest a reduction in the rate constant for electron transfer and is an indication of a less reliable analytical signal for electroanalysis.

traditional drop-casting approaches. EDC/NHS chemistry is often used to link –OH to amines, while silyl-based linkers are also preferred in some cases, as well as the use of self-assembled monolayers using gold–sulfur interactions. Non-specific binding sites are commonly filled using blocking agents such as BSA and ethanolamine. The combination of these elements allows electrodes to be built that are viable to selectively detect target species without interference, for use in complex matrices, and having long lasting storage capability. The advantage of the cross-linking approaches appears to be that they are applicable across a wide range of target species, and they can be used on a range of electrode substrates, both carbon- ITO- and paper-based substrates. If multi-layered electrode designs are required for future analysis, as it appears is the case for complex media such as human serum, then ensuring lack of interference from common biologically relevant analytes (*e.g.*, creatinine and glucose) is key for future designs, as well as ensuring longevity in storage. The latter is probably the biggest challenge for immunosensors at this stage.

3.1.2 Sandwich-type sensors. Sandwich-type sensors come in a variety of forms, using oligonucleotides, antibodies, and aptamers or a combination thereof. They differentiate from other sensor types insofar as the sensor signal is not formed from one singular hybridisation event; rather the target species

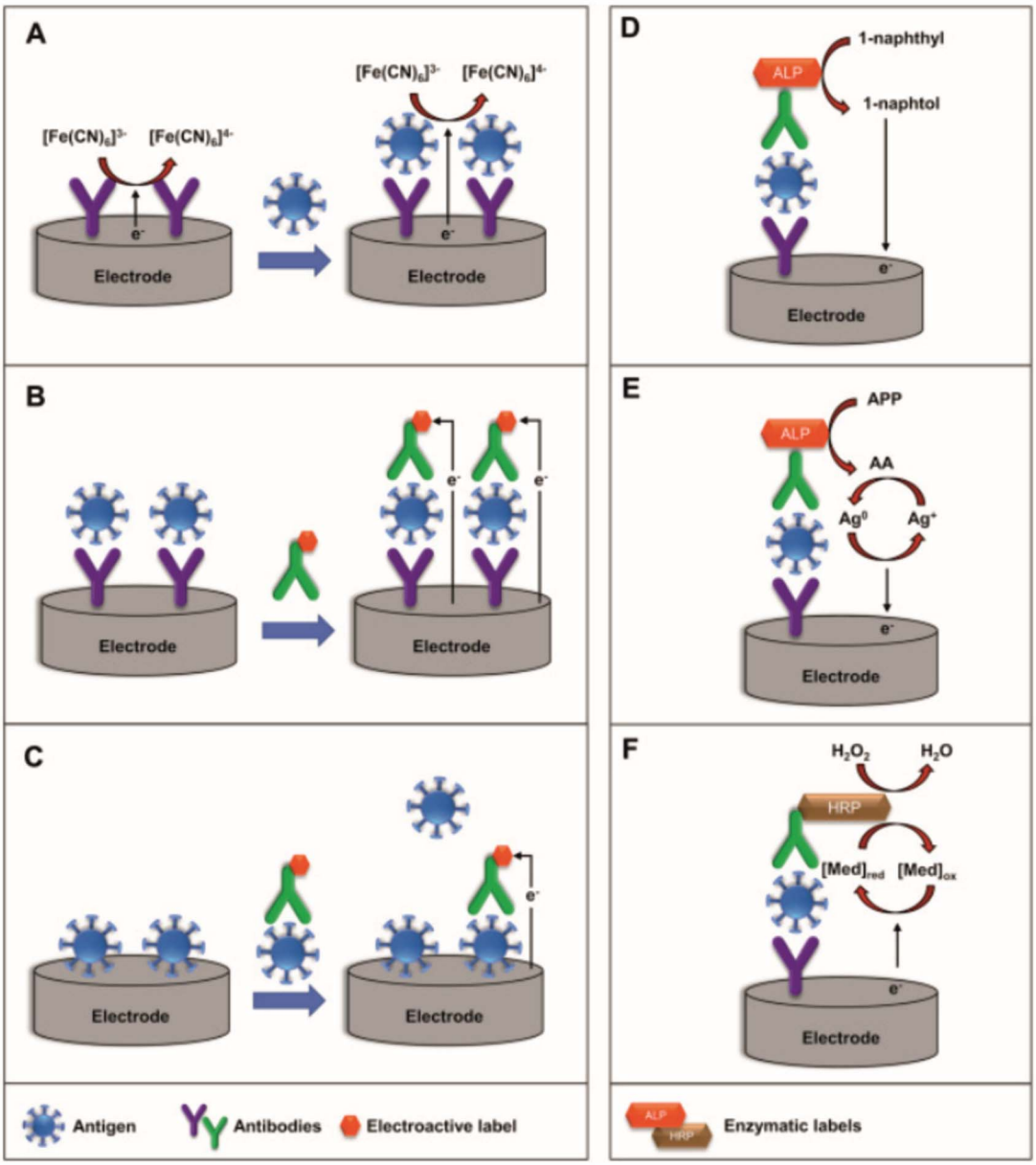

Fig. 5 Schematic representation of (A) label-free, (B) sandwich, and (C) competitive electrochemical immunosensors (left) and schematic representation of the mechanism using enzymatic-labels (right): (D) ALP enzymatic-label for production of electrochemically active 1-naphthol, (E) ALP-catalyzed deposition of electroactive silver, and (F) HRP-catalyzed oxidation of the redox mediator. Reprinted from ref. 36 with permission from Elsevier *via* Rightslink.

is used as a bridge between an electrode substrate and a labelled sensing element, such as an antibody labelled with ferrocene. Fig. 5 depicts the basic differences between immunosensors and sandwich immunosensors.[36] Sandwich-type sensors are more frequently being turned to as a detection strategy in electrochemical biosensing because they offer advantages such as improved target selectivity in real samples, although there is usually a trade-off of increased data acquisition time, while the electrodes are intrinsically complex relative to, for example, immunosensors. Nonetheless sandwich-type sensors are reported with EIS as a detection method in several literature examples since our last review. There are contributions for sandwich-type sensors that target PSA,[37–39] though perhaps EIS is unfavoured as an approach for sandwich-type sensors because most strategies employ electroactive labels that would more beneficially be used in conjunction with voltammetric or amperometric techniques.

Nonetheless, Kavosi *et al.* employ a combined aptamer/immunosensor approach for PSA detection. First, horseradish peroxidase (HRP)-functionalised PSA aptamers are grafted onto dendrimers mounted upon gold nanoparticles, providing a sensory element towards hydrogen peroxide. Second, a glassy carbon electrode is functionalised with PSA antibody and thionine, which acts synergistically as a sensing element towards the HRP-functionalised dendrimer. The aptamer will only hybridise with the electrode substrate in the presence of PSA, which acts as a bridge between the PSA antibody and the PSA aptamer, and this interaction is monitored by observing the reduction of hydrogen peroxide by HRP, which is itself reduced by protonated thionine. The interactions are finely balanced but crucially the whole detection philosophy is reliant upon PSA presence: in the presence of PSA the antibody and aptamer can be bridged together, bringing HRP in close proximity to thionine, resulting in the reduction of hydrogen peroxide. In the absence of PSA during hybridisation, hydrogen peroxide reduction is observed to a much lesser extent. The approach uses EIS to detect PSA to a limit of 5 pg mL^{-1}. It should be noted that the differential pulse voltammetry approach using the same electrode had a lower detection limit of 10 fg mL^{-1} and a wider linear range.

Another example of sandwich-type sensors is reported by Gutiérrez-Zúñiga and Hernández-López who report an electrode exploiting avidin/biotin interactions.[37] Their electrode design incorporates two labelled PSA antibodies: the first PSA antibody is labelled with biotin, which anchors the antibody to the avidin on the electrode surface, while the second antibody is labelled with HRP for an ELISA (confirmatory technique). In the presence of PSA, the two labelled antibodies are bridged by the PSA, creating more resistance at the electrode surface and thus resulting in a higher R_{CT}. This overall electrode design contains many elements and so it is no surprise that the R_{CT} reported are extremely high (in the region of MΩ), but despite this an increase in the resistance is measured using EIS.

There is limited literature using EIS as a quantitative technique for sandwich-type sensors, so perhaps this is either an emerging area, or more likely there are more suitable detection approaches to achieve the best results. Despite this, efforts have been witnessed using nanotechnology (dendrimers and gold nanoparticles) to amplify current signals, while avidin/biotin interactions are also shown to be successful, despite showing very high impedances, which could potentially preclude this as a meaningful analytical approach in combination with EIS.

3.1.3 Aptamer sensors. Aptamer sensors are the second most common type of sensor found to be reported for EIS-based applications since our last review. Instead of using antibodies for the electrolyte-facing component of an aptamer sensor electrode, an aptamer is used instead. There are many types of aptamers and defining the full suite of them is beyond the scope of this review, but summarily aptamers are "small, synthetically derived, single-stranded oligonucleotides which bind to their cognate target with high affinity and selectivity".[40] Aptamers cover quite a broad range materials from which they can be constructed from. A differentiation between oligonucleotide sensors and aptamer sensors is appropriate for this review paper, so henceforth this review assumes that, where oligonucleotide sensors rely solely on a base pair hydrogen bonding for binding, aptamer sensors rely upon more complex non-covalent interactions,[41] involving secondary structures such as multi-branched loops or G-quadruplexes.[40] At least, the property of non-covalent interactions based upon secondary structures of oligonucleotides or peptides appears to differentiate aptamers from oligonucleotides (and potentially peptide-based sensors) themselves. What is certain is that the combination of base pair and structural recognition makes aptamer sensors highly selective and are increasingly employed in sensor development.

Similar to immunosensors, if aptamer sensors are to be employed more widely using EIS as a detection method for target binding, then the aptamer-based electrodes need to be selective and exhibit long term stability. Aptamers are widely considered to be more stable than immunosensors, but still require complex electrode design to anchor the aptamer to the electrode surface to ensure effective connection to the electrode for signal generation, and for long term stability. As will be seen, the approaches utilised to construct aptamer sensors have significant crossover with that of immunosensors.

Table 3 lists the selected works found using the systematic review process. Previously mentioned was a comparative study between an immunosensor and aptamer sensor for the detection of PSA.[42] The authors argue that the aptamer displayed better characteristics in terms of storage capability. An interesting point to note from their work was the change in EIS profile between the aptamer and immunosensor. Fig. 6 depicts EIS profiles for (A, B) an aptamer and (C, D) immunosensor, which display different characteristics. In the case of the aptamer sensor (A, B) for PSA, the impedance profile shows clearly that there are two time constants in the Nyquist plot within the frequency range 0.1–10 000 Hz, one with a large R_{CT} in the high frequency zone, while there is a second time constant with a small R_{CT} within the low frequency zone. This is modelled as two Randles circuits in series, with significantly differing magnitudes. The authors ascribe the two time constants observed to two different charge storage phenomenon: one time constant reflecting charging between the electrode surface and the electrolyte, and a second time constant

Table 3 A table of selected examples of aptamer sensors that employ EIS as the recognition technique

Year	Medium	Electrode	Target	Remarks	Ref.
2020	Human serum	Paper, graphene, PEDOT/PSS,[a] APTMS, SA,[b] CEA aptamers	Carcinoembryonic antigens	Authors remark that the paper-based approach could be useful for early diagnosis and operable by non-specialists	84
2019	Human serum, tears, urine, egg white, wine	SPE, amino-rGO,[c] aminosilica nanoparticles, GLA,[d] lysozyme aptamer	Lysozyme	High stability and linearity with respect to lysozyme. Compatible in many matrices and a wider linear range with EIS compared to potentiostatic methods	44
2019	Aqueous solutions	Au, ISC,[e] MCH,[f] PEX-14 aptamer	Matrix metalloproteinase-14	The authors compare the unlabelled EIS approach, to a labelled approach using tagged ferrocene as a redox probe. The unlabelled approach is reported to have a 10× lower limit of detection	45
2018	Serum, urine, egg white, wine	GC, rGO, MWCNT, chitosan, carbon quantum dots, lysozyme aptamer	Lysozyme	Drop-casted electrode may give rise to long term stability issues	85
2018	Human serum	SPE, GQD, AuNR, anti-PSA	Prostate specific antigen	Sensor can also be modified into an immunosensor but authors argue that aptamer sensor offers advantages in terms of stability	42
2017	Human serum and plant extracts	GC, AuNP, MPA,[g] tubulin	Vinblastine	SEM images show clearly how the tubulin binds to the AuNP/MPA scaffold	86
2016	Aqueous solutions	Interdigitated Au, SH-PEG-COOH, octapeptide, BSA	Proteases (*e.g.* thrombin)	Smartphone controlled electrochemical measurements are the unique aspect – BSA also detected via an immunosensor approach by housing anti-BSA within to a nitrocellulose membrane, casted onto a screen-printed electrode	77
2015	Wine	SPE, DAZ,[h] LysCOX or LysTRAN[i]	Lysozyme	Electrode design uses diazonium coupling, which appears to be less often witnessed than self-assembly, electrodeposition, drop-casting or EDC/NHS chemistry	46
2015	Aqueous solutions	Au, thiolated aptamer	Peanut allergen	Authors note poor stability of electrode if pH is higher than 7	87

[a] (3,4-Ethylenedioxythiophene) : poly(styrenesulfonate). [b] Succinic anhydride. [c] Amine-functionalised reduced graphene oxide synthesized *via* the Hummers' method. [d] Glutaraldehyde. [e] ISC is an amino-functionalised peptide called IS4: (IS4)–$(CH_2)_6$–Cys–OH. [f] Likely to be 6-mercapto-1-hexanol, though the paper is unspecific. [g] 3-Mercaptopropionic acid. [h] The diazonium coupling reaction occurs through the reaction of 4-aminobenzoic acid with $NaNO_2$ in the presence of 0.5 M HCl. [i] Two different aptamers for lysozyme.

reflecting charging between the electrode surface and the electrode modification (*i.e.* the SPE, GQD, AuNR and PSA aptamer, see Table 3 for definitions). Furthermore, it is evident that the R_{CT} of the aptamer sensor overall is twice that of the immunosensor (see *x*-axis on Fig. 6), while the slight uptick in the semicircle in the low frequency zone of the immunosensor Nyquist plot validates the use of the Warburg element (especially for lower concentrations, though perhaps diffusional impedance dissipates thereafter), demonstrating that the immunosensor electrode modification permits the redox probe to interact with the underlying electrode (or its connected modifications, *e.g.* GQD or AuNR) to a much greater extent than the aptamer sensor. The phenomenon could provide a telling difference between aptasensors and immunosensors in terms of permissibility of the electrolyte to the underlying electrode surface: the larger aptasensors provide a sufficient enough barrier that eclipses the impedance contributions observed with respect to diffusional impedance, while immunosensors still show diffusional impedance especially at low concentrations of target analyte.

As with other electrochemical detection strategies, for them to be of any real clinical use they should be designed as point-of-care systems where the measurement can be taken to the patient. Aptamer sensors are no different, since using

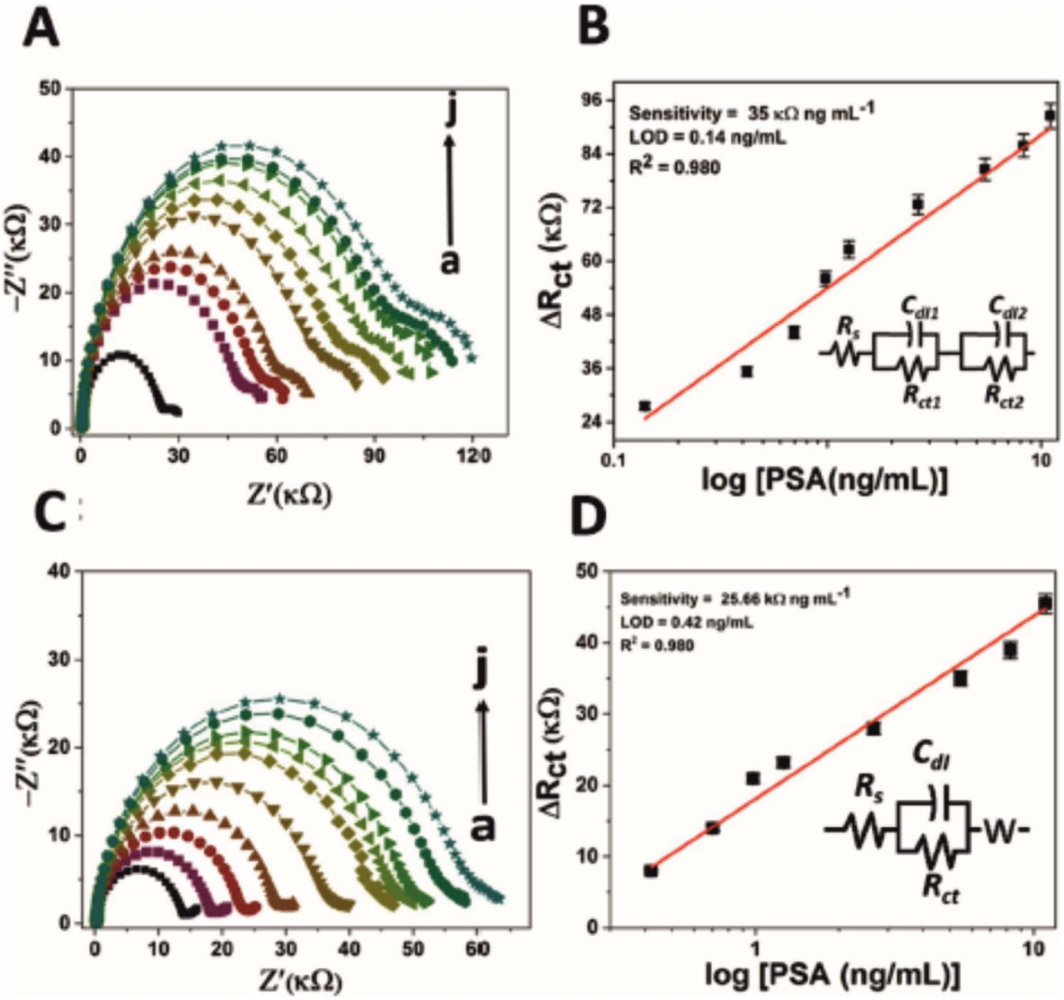

Fig. 6 Nyquist plot for impedance measurement and corresponding calibration curve of (A and B) PSA-aptamer and (C and D) anti-PSA modified electrodes in the presence of different concentration of PSA (0 to 11.06 ng mL^{-1} as shown here as 'a' to 'j') in PBS (pH 7.4) containing 5 mM $[Fe(CN)6]^{3-/4-}$. Of particular interest is the second time constant evident within (A) (small semicircle on the right), which has been modelled as two Randles circuits in series (B). Image reprinted without editing (caption edited) from ref. 42 under a Creative Commons Attribution 4.0 International License with credit to Srivastava and co-workers listed in ref. 42. To view the license please follow the link: http://creativecommons.org/licenses/by/4.0/.

macroelectrodes would prove to be costly if employed on a large scale. Using SPEs as a cheap disposable alternative has been witnessed for many applications.[43] One approach using SPEs for aptamer sensors is reported by Jamei *et al.*, who use carbon SPEs as a basis for their aptamer sensor to detect lysozyme.[44] In their work, amino-functionalised reduced graphene oxide is grafted with mesosilica nanoparticles and an ionic liquid. The composite produced is drop-casted upon a carbon SPE, dried, then the aptamer is covalently linked to the composite using GA as a linker. Hybridisation with lysozyme increases the R_{CT} of the electrode linearly as a function of lysozyme concentration, while the sensor itself is demonstrated to be useful in a range of media including serum, tears, egg white, urine and wine. The ability for the aptamer sensor to be useful in a range of real samples with acceptable recovery rates shows increased versatility of aptamer-based sensors when compared to other sensor types.

In a completely different approach, the aptamer sensor reported by Ma *et al.* incorporates amino-functionalised peptides as a basis for the sensor design to detect matrix metalloproteinase-14.[45] Their approach uses mechanically and chemically cleaned gold electrodes as a substrate upon which a specific peptide chain (named ISC) is self-assembled upon by drop-casting. After washing, exposed gold parts of the electrode were blocked using 6-mercaptohexan-1-ol, exploiting the spontaneous chemistry between gold and sulphur-containing compounds. Upon hybridisation with the matrix metalloproteinase-14, the electrode was demonstrated to increase its R_{CT} of the $Fe^{2+/3+}$ couple between the concentration ranges of 0.1–10 ng mL^{-1}. Furthermore, a secondary approach labelled the peptide with ferrocene, giving the surface of the modified electrode an electroactive species to monitor hybridisation events. Similarly, the labelled approach is effective in the region of 1–10 ng mL^{-1}. Above 10 ng mL^{-1} the electrode is saturated in both cases.

The final example uses diazonium coupling to immobilise the aptamer to the electrode. In the report by Ocaña and co-workers, carbon SPEs are used as an electrode of choice,[46] for reasons already suggested. To modify the electrode, 4-aminobenzoic acid is converted into 4-diazobenzoic acid by reacting with sodium nitrite in 0.5 M HCl. The diazonium compound is electrodeposited upon the carbon SPE using linear sweep voltammetry, exposing benzoic acid's carboxylic acid group to the electrolyte. This approach appears to be a replacement for the generation of oxygenated species upon a carbon electrode surface, which can be completed using a variety of oxidation methods (*e.g.*, UV/O_3 irradiation, voltammetric cycling in KOH). The carboxylic acid group of benzoic acid is then utilised for EDC/NHS chemistry, allowing coupling of one of two lysozyme aptamers (LysCOX or LysTRAN) to the surface. Ethanolamine and bovine serum albumin are used to block non-specific binding sites. The change in R_{CT} towards $Fe^{2+/3+}$ is evident from the EIS traces reported, while the signal is shown to be dependent on the concentration of lysozyme in the region of 0.1–1.0 μM. The sensors were applied to spiked wine samples, with recovery rates of 94–102% but with % RSDs as high as 15%, inferring that the diazonium coupling approach may have some issues with reproducibility.

Aptasensors, though less frequently researched than immunosensors with EIS as the analytical detection approach, may carry an advantage that the EIS profile is purely dominated by the binding events at the electrode without contributions from diffusion. The aptamer table (Table 3) indicates that aptamers are more frequently designed to be applicable in a range of media, rather than being specific to one, which is surely an advantage of aptamers. The electrode functionalisation methods are similar to immunosensors, using silyl linkers, EDC/NHS chemistry or gold/sulfur chemistry, but diazonium chemistry is also witnessed for aptamer electrode design, albeit with lower reproducibility than other approaches. A notable challenge for aptamer sensors is the application to POC devices. The examples listed in this section and in Table 3 show some application of aptamers to printed electrodes, but using drop-casting and diazonium coupling methods for electrode fabrication is likely to give rise to variability in signal output. Further work in this space would perhaps be beneficial to allow quicker movement of aptamers to marketable POC solutions.

3.1.4 Oligonucleotide sensors. Oligonucleotide sensors are those that take advantage of the selective binding between single strands of DNA (ssDNA) *via* hydrogen bonding between complimentary base pairs to produce an analytical signal. This is an attractive approach for the detection of complex biologically relevant targets because of the combination of strong and specific bonding (an explanation of aptamer differentiation is given in section 3.1.3).[47] The sensor strategy for oligonucleotides is to immobilise a capture probe consisting of ssDNA upon an electrode. The capture probe corresponds to a sequence of DNA base pairs that are complimentary towards the base pair sequence of the target ssDNA. As with immunosensors and aptamer sensors, one of the major challenges is ssDNA immobilisation to an electrode surface. Many oligonucleotide sensors use gold/sulfur or amine linkage chemistry for immobilisation as previously seen for other sensors, while others use exploit the inherent charge on the phosphate backbone to deposit oligonucleotides onto a positively charged surface.[47] Despite there being relatively few attempts to combine oligonucleotides with EIS as an analytical signalling technique, there have been reports that target species ranging from HPV through to breast cancer markers using EIS as the analytical technique of choice. Table 4 lists the examples found using the search terms for this review (5 papers). This section will briefly discuss one noteworthy example of oligonucleotide sensors that have been reported since our last review.

Detection of the human papillomavirus (HPV) is the subject of the work reported by Avelino *et al.*[48] Their work uses GA as a linking agent to attach aminated ssDNA onto a scaffold constructed from gold nanoparticles and polyaniline (PANI). Their approach utilises sulphur/gold chemistry to form a strong nanocomposite between AuNP/PANI and the underlying Au electrode surface. The aminated ssDNA is anchored to the PANI *via* GA, which in effect provides an electrode surface of AuNP for signal amplification, as well as a selective binding site for the complimentary DNA for HPV. Perhaps the most noteworthy aspect of their work is the claim that the technique can be utilised to differentiate between HPV viruses that carry different levels of oncogenic risk, outlined in Fig. 7. Three factors were plotted among one another: the values of R_{CT}, n, and the constant phase element (CPE). Observed in Fig. 7 is a grouping of values with observed low values of n, corresponding to HPV viruses with high oncogenic risk (HPV16, HPV58, HPV33, HPV31, and HPV45). For uninfected and low oncogenic risk samples the value of n is demonstrated to be higher in all cases, indicating less deviation from ideal capacitive behaviour of the system. These deviations are usually linked to a lack of surface homogeneity, perhaps related in this case to hydrophobic E5 proteins present on high oncogenic risk HPV viruses. Furthermore, the high oncogenic risk viruses are also demonstrated to have a CPE value in the region of 1.4–1.8, compared to in excess of 2.4 for viruses of low oncogenic risk and uninfected samples. Finally, the viruses of high oncogenic risk show grouping of 10–20 kΩ in terms of their R_{CT} values, whereas the uninfected sample show low R_{CT} values which is likely due to lack of complimentary DNA binding, while low oncogenic risk HPV viruses show variable R_{CT} values. The work was conducted on cell swab samples.

EIS is a less established analytical method for oligonucleotide sensors, compared to immunosensors or aptamer sensors. There are some examples, focusing on a range of target species from HPV to lung and breast cancers and all examples use electrode design methods that exploit gold/thiol chemistry or amine cross linking to carboxylic acid groups. It is surprising that more efforts have not been made particularly with ensuring that the ssDNA capture probes are more strongly held to the surface either through a polymeric network or some other matrix. Furthermore, it is probably telling of the physical nature of ssDNA that efforts are not in higher numbers. The inherent physical structure, being a long and thin DNA strand, would make it difficult to occupy a rod-like structure especially if ssDNA chain lengths are high (described superbly by Vogiazi

Table 4 A table of selected examples of oligonucleotide sensors that employ EIS as the recognition technique

Year	Medium	Electrode	Target	Remarks	Ref.
2021	Nasopharyngeal and oropharyngeal swabs	ITO, PPy,[f] AuNPs, cysteamine, capture probe	Covid-19	Sensor lends itself to EIS due to resistive nature of the electrode design	88
2020	Cells from patient swab	Au, AuNP, MPTMS,[a] PANI,[b] capture probe	HPV	Authors claim that EIS can be used to differentiate oncogenic risk by 3D mapping R_{CT} with the value of the constant phase element and n (*i.e.* the correction factor for the CPE)	48
2017	Human serum	GCE, Cys,[c] AuNP, ssDNA	Lung cancer	Sensor likely has poor long term stability	89
2015	Blood	Au, SH-ssDNA	Breast cancer	Direct attachment of thiolated DNA, with non-specific binding sites blocked using MCH[d]. Authors claim linearity over thirteen orders of magnitude, which seems unlikely and certainly unnecessary in practical terms	90
2014	Aqueous	GCE, RGO,[e] NH_2–ssDNA	Amelogenin	Gene used for sex determination for forensic applications	91

[a] 3-Mercaptopropyltrimethylsiloxane. [b] Polyaniline. [c] Cysteamine. [d] 6-Mercapto-1-hexanol. [e] Reduced graphene oxide. [f] Polypyrrole.

et al.[49]), such that the base pairs are potentially unavailable for effective hybridisation (such as if the rods fall over and lay flat on an electrode surface), which could prevent repeatability of oligonucleotide sensors for electrochemical applications. Sensors using antibodies or aptamers may not suffer the same phenomenon due to their large supramolecular structures. A challenge for successful application of oligonucleotides is therefore to ensure that the sensing elements are secure enough to allow for repeatable data collection. Without this, application using EIS and other electrochemical methods may be limited.

3.1.5 Enzymatic sensors. Enzymatic sensors are the final type of sensor in the bio-based category. Even less examples of enzymatic sensors were identified using the search criteria for this review ($n = 2$), so both examples are described in the text without the aid of a table. A further example using proteins is described. Enzymatic sensors in this context are those that exploit the selective binding of enzymes to substrates or coenzymes to produce an analytical signal using EIS. Enzymes are immobilised onto an electrode surface, exposing the enzymes active site as the electrode surface, which in the presence of a target species, should produce an analytical signal due to charge transfer occurring. Perhaps a unique challenge with enzymatic systems is that covalent binding of enzymes often results in the loss of enzyme functionality,[50] which may reduce the effectiveness of previously discussed immobilisation methods for enzymatic sensors.

The first example described is by Muya *et al.* whose focus is on the detection of vanadium[51] in biological samples for medical monitoring applications. The detection philosophy takes advantage of vanadium's role as an inhibitory substance for the enzyme alkaline phosphatase (ALP). In this regard, the relative difference between ALP activity in the presence and absence of vanadium can be monitored using EIS. Gold electrodes are chosen for electrochemical deposition of a polysulfone hydrogel. The hydrogel acts both as an electron mediator and as an anchor for ALP, presumably through physisorption means since the ALP enzyme is drop-casted upon the hydrogel-modified electrode rather than attached using chemical linkers. Upon interaction with vanadium there is a clear increase in R_{CT} monitored using EIS (see Fig. 8), which appears to be linear with respect to vanadium concentration between 0.2–6.0 μM. More interesting is the fact that a second time constant appears to develop on the Nyquist plot as the concentration of vanadium is raised. The second time constant isn't accounted for in the simulations completed for data analysis, despite providing evidence of two separate processes occurring at the surface, potentially indicating attachment or exchange of vanadium ions onto the enzyme, or perhaps movement of the redox probe in or out of the enzyme. There is also the possibility that vanadium is oxidising the hydrogel, since it is in the +5 oxidation state it will have a high oxidising capability.

The second example is by Voitechovič *et al.*, who report an enzymatic sensor capable of using oxidoreductases to specifically target simple organic compounds such as ethanol or glucose.[52] Their approach uses interdigitated electrode arrays as a substrate, modified by performing an oxidative polymerisation on top of the electrode. The polymerisation mixture contains 0.018 M ammonium persulfate, 0.025 M *N*-(*N*′,*N*′-diethyl dithiocarbamoyl ethyl amido ethyl)aniline (AnD), and 0.225 M HCl in 3 : 1 water : acetonitrile. The authors attempt to encase the enzyme into the polymer coating, but this reduces the overall enzyme activity, so drop-casting of the enzyme solution (alcohol dehydrogenase or glucose dehydrogenase) is preferred. The approach is successful for the detection of ethanol and glucose, measured by observing reductions in the R_{CT} of the enzymatic electrode when in the presence of the target species.

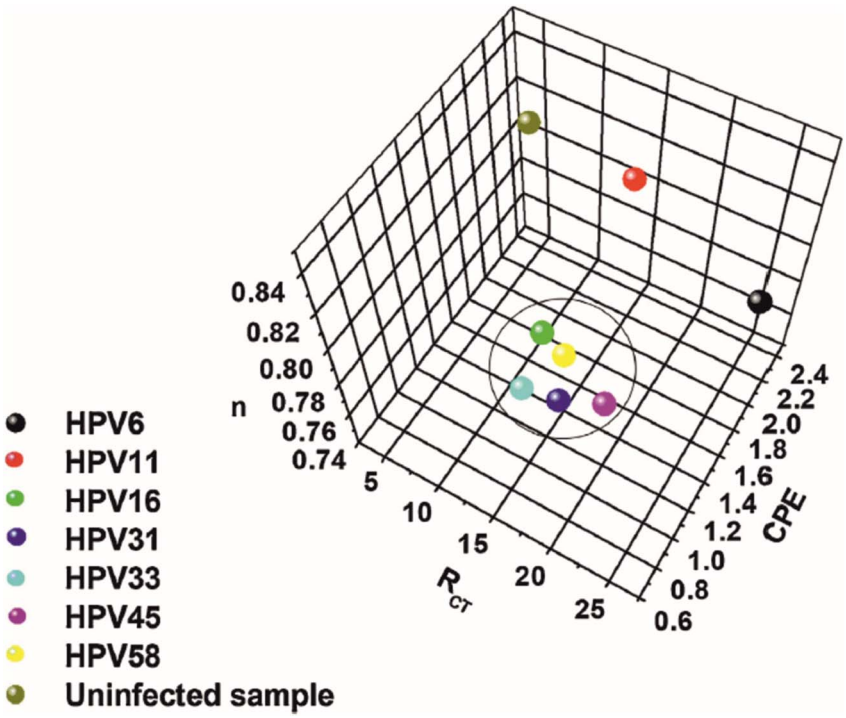

Fig. 7 Three-dimensional plot for the R_{CT}, CPE, and n variables obtained from the theoretical simulation of the Nyquist spectra. Image and caption reused from ref. 48 with permission from Elsevier *via* Rightslink.

Another effort of note is not an enzyme sensor *per se* but it is a protein–ligand interaction approach for the detection of cell signalling proteins by Chung and co-workers.[53] Using glassy carbon electrodes, gold nanoparticles and TBA (2,2′:5′,2″-terthiophene-3′(*p*-benzoic acid)) are electropolymerized onto the electrode surface. EDC/NHS chemistry is used to graft a receptor molecule, named CXCR2, to the surface. This receptor molecule functions biologically to specifically seek chemokine ligands, which themselves are used as biomarkers for certain cancers. The impedimetric sensor showed selectivity in human serum towards CXCL5 ligands in a linear range of 0.1–10.0 ng mL^{-1}, and a detection limit of 0.078 ng mL^{-1}.

Enzymatic sensors appear to be less well researched using EIS. There are many examples of enzyme systems used electrochemically but normally amperometric methods are chosen to observe increases in oxidative current. In theory, an increase in oxidative current would lend itself to changes in R_{CT}, and therefore render EIS as a useful method for the determination of target species. However, there does appear to be potential complications with EIS (*i.e.*, the unexplained appearance of a second time constant when in the presence of an enzyme inhibitor). Perhaps EIS could be a technique of choice for enzymatic sensors if complex physical processes when enzyme meets analyte were further de-convoluted through further research.

3.2 Non-bio-based sensors

Non-bio-based sensors are defined in this review as sensors that have been designed without the use of a natural (or synthetic natural) molecule as part of the electrode design. This includes any sensors that are designed using molecularly imprinted polymers, or nanocomposites without the use of proteins, antibodies, enzymes or DNA nucleotides. Using the specified search criteria, 15 examples of non-bio-based sensors were identified that incorporated EIS as the quantification technique. Of these 15, 8 of them are termed as "composite" sensors, 6 as "molecularly imprinted polymer" sensors, and 1 is a direct detection method. This section will discuss these non bio-based sensors and determine whether there are any favoured approaches in the design and implementation of non bio-based sensors.

3.2.1 Composite sensors. Composite sensors in this context are quite broad in definition and are essentially treated in this review as any non bio-based detection strategy that doesn't make use of molecularly imprinted polymers. This treatment is purely for simplicity in this review and is unlikely to reflect sensor types beyond this review. Composite sensors normally incorporate nanomaterials, such as graphene or dendrimers, and the detection philosophies are varied in approach. There are examples discussed below of sensors utilising ionophore interactions, through to metal-ion affinity interactions in the authors quest to design detection strategies without using biological molecules. Once again, a large number of composite sensors are reported that use EIS, but it is normally employed as a method to confirm successful immobilisation of substances upon electrode surfaces rather than an analytical technique. This section only lists those reports that use EIS as the analytical signal. A list of the most recent

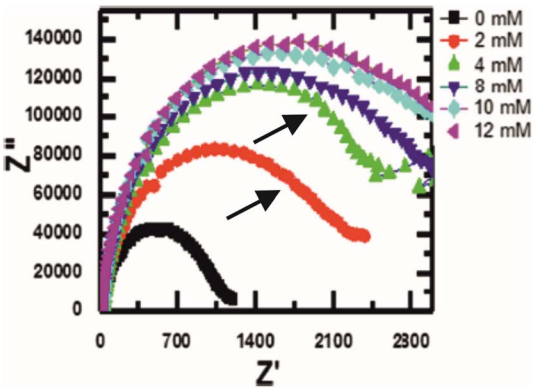

Fig. 8 Nyquist plot of an alkaline phosphatase electrode in the presence of vanadium. Note how there is a second, albeit small, time constant appearing after the introduction of vanadium (indicated by the black arrows). Figure obtained and reused from ref. 51 with permission from Springer *via* Rightslink.

examples of composite sensors using EIS as an analytical technique is presented in Table 5.

Salivary calcium analysis is the topic of focus in the work by Magar *et al.*[54] Their approach makes use of 4-aminothiophenol self-assembled upon gold electrodes, providing an amino group functionality for EDC/NHS coupling of an ionophore to the electrode. Ionophores are useful for selective sensors because they are specifically designed to permit the passage of selected ions. In the work by Magar *et al.*, they synthesize an ionophore specific to Ca^{2+} ions through the reaction of benzil with 4-aminosalicylic acid, under reflux conditions. The result is an electrode with improved wettability, which undoubtedly helps migration of Ca^{2+} ions into the inner Helmholtz plane under negative electrode biases, facilitated and coordinated by the ionophore. The supplementary data also suggests that the electrode offers no change in R_{CT} when subjected to Mg^{2+}, Co^{2+}, Cu^{2+}, Ba^{2+}, K^{+}, Na^{+}, Li^{+}, and NH_4^{+}, which offers some promise, although none of these ions are comparable in m/z ratio, with notable omissions from Ag^{2+}, Hg^{2+} and Cd^{2+}, which could represent a fairer comparison for selectivity. Despite this, the authors report a linear range over five orders of magnitude (1.0×10^{-11} to 1.0×10^{-6} M), with a limit of detection of 3.5×10^{-12} M.

Non-bio-based detection platforms have also been developed for whole cell detection. Dervisevic and co-workers,[55] report an interesting method combining self-assembled monolayers, dendrimers, ferrocene, and folic acid (FA) or 3-amino phenylboronic acid (BA). Using a gold electrode with self-assembled cysteamine, ferrocene-cored polyamidoamide (PAMAM) dendrimers are cross-linked to cysteamine using GA as a linker. A modification of either FA or BA completes the electrode, which acts as the whole cell binding site through differing mechanisms. For the FA electrode, the philosophy is derived from the over-expression of the folate receptor in cancerous cells, so making FA the sensing element on the electrode is targeting the folate receptor on a cell surface. For the BA electrode, the approach exploits the fact that sialic acids (SAs) are present on tumour surfaces in large amounts. The hydroxyl groups on boronic acid are situated favourably to chelate the SA produced by cancerous cells. Both approaches report success in whole cell detection. They exhibit a detection linear range of 1.0×10^2 to 1.0×10^6 cells per mL, with the FA electrode showing a slightly

Table 5 A table of composite sensors using EIS as the detection technique

Year	Medium	Electrode	Target	Remarks	Ref.
2022	Aqueous	GCE, CuO-NPs,[p] PANI-Mu[q]	Cholesterol	Diffusionless EIS profile	92
2021	Aqueous	GCE, AuNPs, MCH,[n] BA[o]	Glucose	Dual detection sensor, with DPV being slightly more sensitive in terms of limit of detection	93
2021	Blood	SS,[a] AuNP, SH-β-cyclodextrin	Low density lipoprotein	Unusual substrate	94
2021	Aqueous	Pt, crown ether	New psychoactive substances	Crown ether stability likely to present problems for long term storage	95
2020	Saliva	Au, 4ATP,[b] ionophore[c]	Calcium	Encouraging results with pM detection limit and pM to μM range but has long term stability issues	54
2017	Cells	Au, CYS,[d] PAMAM,[e] ferrocene, FA/BA[f]	Cancer cells	Detection of whole cancer cells is possible using the approach to a detection limit of 20 cells per mL	55
2015	Egg white	GCE, AuNP, ME,[g] CPTMS,[h] IDA,[i] Cu	Lysozyme	Sensor uses metal ion affinity interactions to target lysozyme	56
2015	Artificial serum	Au, MTS,[j] CGNP,[k] PDDA[l]	BSA[m]	Two dimensional silica network (MTS) shows very high resistance to charge transfer, yet further modifications significantly reduce this	96

[a] Stainless steel. [b] 4-Aminothiophenol. [c] In-house synthesized ionophore made from the reflux of benzil and 4-amino salicylic acid for 6 h in methanol and toluene-4-sulfonic acid. [d] Cysteamine. [e] Polyamidiamine dendrimers. [f] Two electrodes were studied, one used folic acid (FA) and the other used 3-amino-phenylboronic acid (BA). [g] 2-Mercaptoethanol. [h] 3-Chloropropyl trimethoxysilane. [i] Iminodiacetic acid. [j] 3-Mercaptopropyl triethoxysilane. [k] Citrate-capped gold nanoparticles. [l] Poly(diallyldimethylammonium chloride). [m] Bovine serum albumin. [n] Mercaptohexanoic acid. [o] Boronic acid. [p] Copper oxide nanoparticles. [q] Polyaniline with murexide.

better limit of detection (28 cells mL^{-1}) compared to the BA electrode (20 cells mL^{-1}).

A final noteworthy approach for composite-based sensors takes advantage of metal-chelate affinity interactions, which are normally exploited in chromatographic experiments. The interactions are essentially metal–ligand coordination interactions between metal ions and chelating moieties on the surface of amino acids. Arabzadeh and Salimi report on their approach,[56] which asserts femtomolar level detection of lysozyme using EIS. The metal-affinity interactions in the case of lysozyme are between Cu^{2+} ions and the amino acid chain of lysozyme, which contains a number of chelating ligands including iminodiacetic acid (IDA). The electrode is fabricated by electrodepositing AuNPs on a glassy carbon surface, which are then self-assembled with 2-mercaptoethanol before further modification with 3-CPTMS. The IDA is then chemically bonded to the electrode by displacement of the chlorine from 3-CPTMS, leaving two carboxylic acid groups available on the electrode surface. The final step is to chelate the IDA with Cu^{2+}, derived from $CuSO_4$, to provide the electrode surface with a series of copper ions available for interaction with the lysozyme amino acid chains. The resulting electrode successfully detects lysozyme in egg white within a linear range of 0.1 pM to 0.1 mM.

Composite sensors have a broad scope in this context and therefore a variety of strategies are used for selectivity, such as ionophores or metal-chelate interactions. The fabrication approaches remain the same, however. Composites may be important to reduce cost because complex biomolecules are not used for sensor design, but more often it would seem that EIS is unfavoured as an analytical detection method. The reason for this is unclear from the examples presented. In all cases EIS has been successfully employed the generate the analytical signal so there is no reason why EIS cannot be employed for more cases, especially in cases that require low detection limits and wide linear ranges.

3.2.2 Molecularly imprinted polymer sensors. The final group of sensors discussed in this review are those of molecularly imprinted polymer (MIP) sensors. MIPs encapsulate the target species within a polymer framework, creating a polymer network with target-shaped cavities after removal. The cavities may permit small ions or electrons through, yet if those holes are filled by the target analyte the resistance of the electrode changes. The magnitude of the change can be related to a concentration of target species and monitored analytically using EIS. For more information on MIP sensors, see the reviews by Crapnell.[57,58] There have been a few reports on this approach using EIS to monitor analytical signal; a summary of the examples identified using the search terms for this review is provided in Table 6.

A notable contribution to the technique comes from Trevizan *et al.*, who report the use of MIPs in their sensor for the detection of uric acid (UA),[59] a commonly pursued biologically relevant analyte due to its role in causing many diseases. Using a fluorine tin oxide (FTO) electrode, 10 mM Bismarck brown Y (BBY) is electrodeposited using cyclic voltammetry in the presence of 1 mM UA and 0.5 M KCl. BBY is an azo dye, historically used as a staining agent for cellulose and DNA, though less so in modern times. BBY is reported to undergo radical formation at electrodes, which can terminate as BBY dimers. The process of radical formation *via* electrooxidation is repeated until the polymer covers the electrode, encapsulating the UA molecule, which is removed to leave UA-shaped cavities that preferentially accept UA molecules for electrode selectivity. A notable difference with the detection approach in this instance is the lack of need for a redox couple such as $Fe^{2+/3+}$. With UA being electroactive itself, it undergoes charge transfer reactions when captured by the MIP cavities, hence in the presence of a larger amount of UA, the MIP sensor should show an enhanced level of UA oxidation, and therefore a lower R_{CT} (*i.e.* a lower *V*/*I* ratio). Interestingly, this is only partially the case, because according to

Table 6 A table of molecularly imprinted polymer sensors using EIS as the detection technique

Year	Medium	Electrode	Target	Remarks	Ref.
2021	Aqueous	FTO,[a] ABBY[b]	Uric acid	The polymer is conductive and stores charge – no redox probe is needed for a signal	59
2021	Egg white	μAu, doped PPY,[c] chitosan, GLA[d]	Lysozyme	Use of a cobaltabis in the polymer layer eliminates charge imbalance	60
2021	Serum	SPE,[e] 2-AMP[f]	Galectin-3	Capacitance used as an analytical measurement	97
2019	Food	AuSPE,[g] Po-PD[h]	Deoxynivalenol	Target species identified in cornflakes and could lead to gastrointestinal disorders	98
2018	Serum	SPE, PEDOT,[i] PEBT[j]	BSA[k]	Control without PEDOT shows 9× less sensitivity	99
2018	Aqueous	Pt, ADMA,[l] F.Crown,[m] F.Carboxy,[n] CL,[o] TBAP[p]	ADMA	No significant difference in LoD between differential pulse voltammetry and EIS	100

[a] Fluorine tin oxide. [b] Poly(azo-Bismarck brown Y). [c] Poly(pyrrole) doped with $Cs[3,3\text{-}Co(1,2\text{-}C_2B_9H_{11})_2]$. [d] Glutaraldehyde. [e] Carbon screen-printed electrode. [f] 2-Aminophenol. [g] Gold screen-printed electrode. [h] Poly(*o*-phenylenediamine). [i] Poly(3,4-ethylenedioxythiophene). [j] Poly(Eriochrome Black T). [k] Bovine serum albumin. [l] Asymmetric dimethylarginine. [m] Bis(2,2′-bithien-5-yl)-methylbenzo-18-crown-6. [n] *p*-Bis(2,2′-bithien-5-yl) methylbenzoic acid. [o] 4,4′-Bisthiophene-3-yl-5,5′-bisthiophene-2-yl-3,3′-(2,2′-bithiophene). [p] Tetrabutylammonium perchlorate.

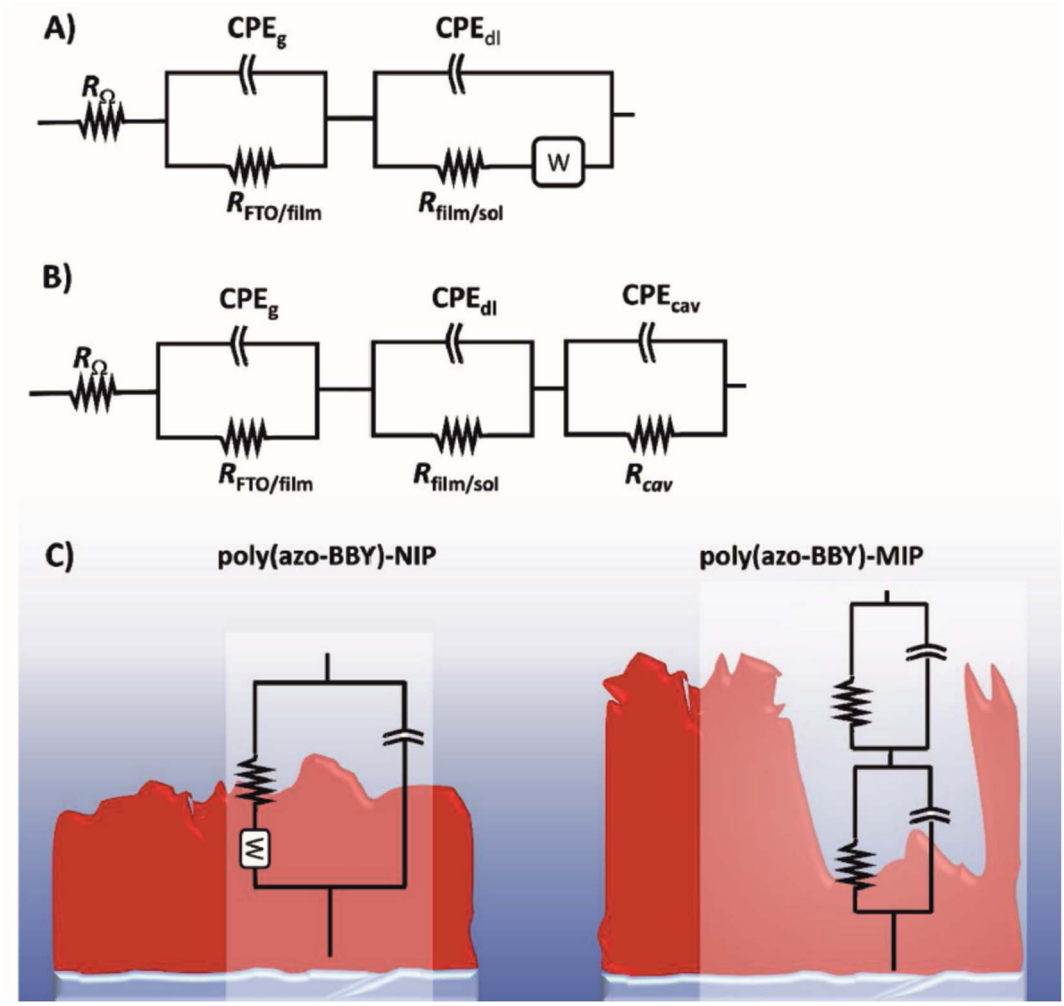

Fig. 9 EIS circuit models for (A) non molecularly imprinted polymer, (B) molecularly imprinted polymer, and (C) a diagram of the NIP and MIP, with an explanation of where each circuit component corresponds to. Reprinted from ref. 59 with permission from Elsevier *via* Rightslink.

their circuit model there are multiple charge transfer processes occurring, outlined in Fig. 9, which depicts a model for how the individual circuit elements reflect the physical processes occurring. Despite this philosophical approach to modelling, there appears to be overlap of time constants within their experimental data, since having three individual elements to model the full system should show three discreet processes occurring on a Nyquist plot, but this is not the case in their work. Perhaps overlapping time constants is a reason why the authors choose capacitance as the analytical signal later in the paper, because it is clear that the cavities display increased charging with respect to UA concentration, with a high degree of reliability.

Following from the previous point regarding multiple time constants, Zouaoui and co-workers themselves use MIPs in their work to detect lysozyme in egg white.[60] In their work, two time constants are clearly identifiable on the Nyquist plots. Yet this may be due to their intrinsic electrode design. The approach first deposits polypyrrole (PPY) on the surface, then chitosan mixed with lysozyme (LYS) is electrodeposited on top of the PPY layer. Hence, due to an extra layer of electrode modification to improve the adhesion of chitosan to the electrode, the second time constant may be due to this addition. The approach allows for LYS detection over 5 orders of magnitude (10^{-11} to 10^{-6}) with a limit of detection of 5×10^{-12} M.

There are a limited number of MIP papers presented in this review, and quite clearly the electrode fabrication processes are markedly different for MIPs than all other types presented, because they don't use gold/sulfur or amine linkage chemistry or blocking agents as with other types of sensors. They also offer solutions that directly oxidise target species without the need for redox probes, which is seldom seen for other EIS-based sensors. MIPs can encapsulate both small molecules and complex molecules, whereas immunosensors, aptasensors and oligonucleotide sensors are more suited towards complex molecules. Perhaps MIP sensors might benefit from some further work examining the equivalent circuit models for MIP-based approaches, because there are clearly some praise-worthy efforts to model EIS traces, but more work would bolster understanding to improve confidence in the use of EIS as an analytical detection method.

3.3 Summary

Our previous review examined EIS from its conception through to applications as of 2013, finding that it was primarily employed as a technique to support voltammetric evidence rather than one that is used front-and-centre for analytical detection of substances. We surmised that there was a clear scope for use in bioanalysis and that low detection limits in the picomolar range were already being reported in immunosensor applications.

Presently, it can be remarked that EIS is still primarily used as a supplementary technique for electrode characterisation, but despite this there are several papers that exploit the full potential of EIS as an analytical technique, in particular for immunosensors. Through smart electrode design that incorporates cross-linking chemistries to create strong bonds between substrate and antibody, immunosensors are now being reported for over 25 different targets alone in this review, some with detection limits in the femtomolar range. SPEs, and more recently, paper-based substrates are increasingly commonplace as the field recognises the need to scale the technique into something more practical such as a handheld device for detection with disposable electrodes. Ensuring lack of interference from other biologically-relevant analytes will be key for future immunosensors especially when using more transferable and portable devices using printed electrodes and paper substrates. Aptasensors are too witnessing attention by researchers while using EIS as a technique, and this review has highlighted a potential idea that complex aptamer structures remove diffusional impedance components from EIS experiments, potentially simplifying both equivalent circuit modelling and overall data analysis. Aptamer-based sensors also appear to be more versatile in terms of matrix effects. In other words where many sensors are tailored towards one matrix (*i.e.*, aqueous, serum, blood *etc.*), aptamer-based sensors appear to be less affected by matrices, which makes them applicable within a wider range of environments. Some aptasensor electrode fabrication methods show large variability, so when designing future electrodes for point-of-care diagnostics it will be vitally important that the variability is limited for accurate point-of-care testing. Oligonucleotide sensors are less common, likely as a result of the physical nature of oligonucleotides making the electrochemical responses difficult to control. Ensuring control of the sensing element to reduce inter-electrode variability is a big challenge for oligonucleotide sensors for all electrochemical applications. Enzymatic sensors are sparsely researched for EIS. This may be due to the difficulties in immobilising enzymes to substrates, which require non-covalent interactions to ensure enzyme functionality isn't lost, though this could compromise on longevity. De-convoluting EIS profiles for enzymatic sensors may give way to some enhanced mechanistic information on the nature of enzymes in electrochemical environments so EIS should not be discounted, especially in studies of a fundamental or qualitative nature.

Other works have made efforts to circumvent the use of biomolecules in sensor designs, while still attempting to target analytes within physiological environments, using composite electrodes or MIPs. Composite electrodes tend to use similar cross-linking chemistries to bio-based electrodes but use synthetic ionophores or metal-chelate interactions as the selectivity elements. This does give rise to what appears to be a more varied range of targets (complex and simple molecules) whereas the bio-based group of electrodes appears to focus ostensibly on complex molecules. Further work on composite sensors could explore a wider range of target analytes, identify selective electrodes for small molecules and ions and de-convolute EIS profiles obtained to determine mechanisms of interaction between electrodes and substrates. MIPs offer a completely different approach towards EIS sensor design but more work on successful circuit modelling may be appropriate for MIPs to improve user confidence in the technique. The range of targets using MIPs once again appears more varied. Perhaps the wider applicability between simple and complex molecules differentiates the bio-based and non-bio-based approaches somewhat.

Since our last review it is fair to state that there have been significant advances in electrode designs to ensure electrodes are more selective, less prone to matrix effects, and have longer storage capacities. It would also be fair to suggest that the technique has seen an uptick in use, while also recognising that voltammetric and amperometric sensors are still the favoured approach for all sensor types. De-convoluting EIS profiles in a generic way for each sensor platform might be a valuable contribution to the field to pave the way for EIS as a choice technique, which could in theory prove to be more sensitive than other electrochemical methods, while simultaneously offering more mechanistic insight into the true nature of electrode processes.

Conflicts of interest

There are no conflicts of interest to report.

References

1 E. P. Randviir and C. E. Banks, *Anal. Methods*, 2013, **5**, 1098–1115.
2 E. P. Randviir, *Electrochim. Acta*, 2018, **286**, 179–186.
3 A. J. Bard and L. R. Faulkner, *Electrochemical Methods: Fundamentals and Applications*, John Wiley & Sons Inc., USA, 2nd edn, 2001.
4 J. E. B. Randles, *Discuss. Faraday Soc.*, 1947, **1**, 11–19.
5 B. Breyer and F. Gutmann, *Trans. Faraday Soc.*, 1946, **42**, 645–654.
6 F. Ciucci, *Curr. Opin. Electrochem.*, 2019, **13**, 132–139.
7 H. M. Hashem, S. S. M. Hassan, A. H. Kamel, A. E.-G. E. Amr and E. M. AbdelBary, *Polymers*, 2020, **12**, 673.
8 I.-A. Stoian, B.-C. Iacob, C.-L. Dudaş, L. Barbu-Tudoran, D. Bogdan, I. O. Marian, E. Bodoki and R. Oprean, *Biosens. Bioelectron.*, 2020, **155**, 112098.
9 C. Tortolini, E. Capecchi, F. Tasca, R. Pofi, M. A. Venneri, R. Saladino and R. Antiochia, *Nanomaterials*, 2021, **11**, 718.

10 M. L. Yola, N. Atar and N. Özcan, *Nanoscale*, 2021, **13**, 4660–4669.
11 M. L. Yola and N. Atar, *Anal. Bioanal. Chem.*, 2021, **413**, 2481–2492.
12 R. A.-O. Couto, C. Coelho, B. Mounssef Jr, S. F. A. Morais, C. D. Lima, W. A.-O. Dos Santos, F. A.-O. Carvalho, C. A.-O. X. Rodrigues, A. A.-O. Braga, L. A.-O. X. Gonçalves and M. B. Quinaz, *Nanomaterials*, 2021, **12**(3), 353.
13 L. C. Lopes, D. Lima, A. C. Mendes Hacke, B. S. Schveigert, G. N. Calaça, F. F. Simas, R. P. Pereira, M. Iacomini, A. G. Viana and C. A. Pessôa, *Talanta*, 2021, **223**, 121634.
14 H. Karimi-Maleh, M. Alizadeh, Y. Orooji, F. Karimi, M. Baghayeri, J. Rouhi, S. Tajik, H. Beitollahi, S. Agarwal, V. K. Gupta, S. Rajendran, S. Rostamnia, L. Fu, F. Saberi-Movahed and S. Malekmohammadi, *Ind. Eng. Chem. Res.*, 2021, **60**, 816–823.
15 A. Ghoorchian, A. Afkhami, T. Madrakian, R. Rameshan, C. Rameshan and A. Hajian, *Sens. Actuators, B*, 2020, **324**, 128723.
16 P. A. Pushpanjali, J. G. Manjunatha and M. T. Srinivas, *FlatChem*, 2020, **24**, 100207.
17 T. T. Hien Ngo, I. C. Fort, T. H. Pham and G. L. Turdean, *Electroanalysis*, 2021, **33**, 323–335.
18 L.-E. Gliga, B.-C. Iacob, B. Cheşcheş, A. Florea, L. Barbu-Tudoran, E. Bodoki and R. Oprean, *Electrochim. Acta*, 2020, **354**, 136656.
19 D. Ghanei Agh Kaariz, E. Darabi and S. M. Elahi, *J. Theor. Appl. Phys.*, 2020, **14**, 339–348.
20 R. A. S. Couto, B. Mounssef, F. Carvalho, C. M. P. Rodrigues, A. A. C. Braga, L. Aldous, L. M. Gonçalves and M. B. Quinaz, *Sens. Actuators, B*, 2020, **316**, 128133.
21 N. Manjula, V. Vinothkumar, S.-M. Chen and A. Sangili, *J. Mater. Sci.: Mater. Electron.*, 2020, **31**, 12595–12607.
22 M. Ognjanović, D. M. Stanković, M. Jović, M. P. Krstić, A. Lesch, H. H. Girault and B. Antić, *ACS Appl. Nano Mater.*, 2020, **3**, 4654–4662.
23 M. Rahimi-Nasrabadi, F. Ahmadi, H. Beigizadeh, M. S. Karimi, A. Sobhani-Nasab, Y. Joseph, H. Ehrlich and M. R. Ganjali, *Microchem. J.*, 2020, **154**, 104654.
24 N. Farvardin, S. Jahani, M. Kazemipour and M. M. Foroughi, *Anal. Methods*, 2020, **12**, 1767–1778.
25 T.-W. Chen, S. Chinnapaiyan, S.-M. Chen, A. Hossam Mahmoud, M. S. Elshikh, H. Ebaid and M. Taha Yassin, *Ultrason. Sonochem.*, 2020, **62**, 104872.
26 Y. Y. Yilmaz, E. E. Yalcinkaya, D. O. Demirkol and S. Timur, *Sens. Actuators, B*, 2020, **307**, 127665.
27 Y. Duan, N. Wang, Z. Huang, H. Dai, L. Xu, S. Sun, H. Ma and M. Lin, *Mater. Sci. Eng., C*, 2020, **108**, 110501.
28 H. Ben Halima, F. G. Bellagambi, A. Alcacer, N. Pfeiffer, A. Heuberger, M. Hangouët, N. Zine, J. Bausells, A. Elaissari and A. Errachid, *Anal. Chim. Acta*, 2021, **1161**, 338468.
29 M. Aydın, E. B. Aydın and M. K. Sezgintürk, *Biosens. Bioelectron.*, 2018, **117**, 720–728.
30 X. Li, Z. Qin, H. Fu, T. Li, R. Peng, Z. Li, J. M. Rini and X. Liu, *Biosens. Bioelectron.*, 2021, **177**, 112672.
31 Y. Castaño-Guerrero, F. T. C. Moreira, A. Sousa-Castillo, M. A. Correa-Duarte and M. G. F. Sales, *Electrochim. Acta*, 2021, **366**, 137377.
32 N. Tarimeri and M. K. Sezgintürk, *Electroanalysis*, 2020, **32**, 1065–1074.
33 O. K. Adeniyi and P. N. Mashazi, *Electrochim. Acta*, 2020, **331**, 135272.
34 E. Burcu Aydın, *Int. J. Environ. Anal. Chem.*, 2020, **100**, 363–377.
35 E. B. Aydın, M. Aydın and M. K. Sezgintürk, *Biosens. Bioelectron.*, 2018, **121**, 80–89.
36 L. C. Brazaca, P. L. dos Santos, P. R. de Oliveira, D. P. Rocha, J. S. Stefano, C. Kalinke, R. A. Abarza Muñoz, J. A. Bonacin, B. C. Janegitz and E. Carrilho, *Anal. Chim. Acta*, 2021, **1159**, 338384.
37 G. G. Gutiérrez-Zúñiga and J. L. Hernández-López, *Anal. Chim. Acta*, 2016, **902**, 97–106.
38 G. G. Gutiérrez-Zúñiga and J. L. Hernández-López, *Procedia Chem.*, 2014, **12**, 47–54.
39 B. Kavosi, A. Salimi, R. Hallaj and F. Moradi, *Biosens. Bioelectron.*, 2015, **74**, 915–923.
40 E. M. McConnell, J. Nguyen and Y. Li, *Front. Chem.*, 2020, **8**, 434.
41 A. Ruscito and M. C. DeRosa, *Front. Chem.*, 2016, **4**, 14.
42 M. Srivastava, N. R. Nirala, S. K. Srivastava and R. Prakash, *Sci. Rep.*, 2018, **8**, 1923.
43 A. García-Miranda Ferrari, S. J. Rowley-Neale and C. E. Banks, *Talanta Open*, 2021, **3**, 100032.
44 H. R. Jamei, B. Rezaei and A. A. Ensafi, *Colloids Surf., B*, 2019, **181**, 16–24.
45 F. Ma, Y. Zhu, Y. Chen, J. Liu and X. Zeng, *Talanta*, 2019, **194**, 548–553.
46 C. Ocaña, A. Hayat, R. K. Mishra, A. Vasilescu, M. del Valle and J.-L. Marty, *Bioelectrochemistry*, 2015, **105**, 72–77.
47 D. C. Ferrier, M. P. Shaver and P. J. W. Hands, *Biosens. Bioelectron.*, 2015, **68**, 798–810.
48 K. Y. P. S. Avelino, L. S. Oliveira, N. Lucena-Silva, C. P. de Melo, C. A. S. Andrade and M. D. L. Oliveira, *J. Pharm. Biomed. Anal.*, 2020, **185**, 113249.
49 V. Vogiazi, A. de la Cruz, W. R. Heineman, R. J. White and D. D. Dionysiou, *Anal. Chem.*, 2021, **93**, 812–819.
50 A. Alshammari, M. G. Posner, A. Upadhyay, F. Marken, S. Bagby and A. Ilie, *ACS Appl. Mater. Interfaces*, 2016, **8**, 21077–21088.
51 F. N. Muya, P. G. L. Baker and E. I. Iwuoha, *Electrocatalysis*, 2020, **11**, 374–382.
52 E. Voitechovič, A. Bratov, N. Abramova, J. Razumienė, D. Kirsanov, A. Legin, D. Lakshmi, S. Piletsky, M. Whitcombe and P. K. Ivanova-Mitseva, *Electrochim. Acta*, 2015, **173**, 59–66.
53 S. Chung, P. Chandra, J. P. Koo and Y.-B. Shim, *Biosens. Bioelectron.*, 2018, **100**, 396–403.
54 H. S. Magar, M. N. Abbas, M. B. Ali and M. A. Ahmed, *J. Solid State Electrochem.*, 2020, **24**, 723–737.
55 M. Dervisevic, M. Şenel, T. Sagir and S. Isik, *Biosens. Bioelectron.*, 2017, **91**, 680–686.

56 A. Arabzadeh and A. Salimi, *Biosens. Bioelectron.*, 2015, **74**, 270–276.
57 R. D. Crapnell, N. C. Dempsey-Hibbert, M. Peeters, A. Tridente and C. E. Banks, *Talanta Open*, 2020, **2**, 100018.
58 R. D. Crapnell, A. Hudson, C. W. Foster, K. Eersels, B. V. Grinsven, T. J. Cleij, C. E. Banks and M. Peeters, *Sensors*, 2019, **19**, 1204.
59 H. F. Trevizan, A. Olean-Oliveira, C. X. Cardoso and M. F. S. Teixeira, *Sens. Actuators, B*, 2021, **343**, 130141.
60 F. Zouaoui, S. Bourouina-Bacha, M. Bourouina, A. Alcacer, J. Bausells, M. Martin, F. Bessueille, S. Minot, N. Jaffrezic-Renault, N. Zine and A. Errachid, *Sens. Actuators, B*, 2021, **339**, 129903.
61 T. Anusha, K. S. Bhavani, J. V. Shanmukha Kumar, P. K. Brahman and R. Y. A. Hassan, *Bioelectrochemistry*, 2022, **143**, 107935.
62 N. Tasić, L. Cavalcante, E. Deffune, M. S. Góes, T. R. L. C. Paixão and L. M. Gonçalves, *Electrochim. Acta*, 2021, **397**, 139244.
63 W. Białobrzeska, D. Firganek, M. Czerkies, T. Lipniacki, M. Skwarecka, K. Dziąbowska, Z. Cebula, N. Malinowska, D. Bigus, E. Bięga, K. Pyrć, K. Pala, S. Żołędowska and D. Nidzworski, *Biosensors*, 2020, **10**, 175.
64 S. Palanisamy, D. Senthil Raja, B. Subramani, T.-H. Wu and Y.-M. Wang, *ACS Appl. Mater. Interfaces*, 2020, **12**, 32468–32476.
65 S. V. de Almeida, J. Cancino-Bernardi, J. K. de Andrade, M. L. Felsner, V. Zucolotto and A. Galli, *Microchim. Acta*, 2020, **187**, 438.
66 K. Mahato, B. Purohit, A. Kumar and P. Chandra, *Biosens. Bioelectron.*, 2020, **148**, 111815.
67 B. Demirbakan and M. K. Sezgintürk, *J. Electroanal. Chem.*, 2019, **848**, 113304.
68 M. N. Sonuç Karaboğa and M. K. Sezgintürk, *Analyst*, 2019, **144**, 611–621.
69 P. Assari, A. A. Rafati, A. Feizollahi and R. Asadpour Joghani, *Mikrochim. Acta*, 2019, **186**, 484.
70 J. Bhardwaj, A. Sharma and J. Jang, *Biosens. Bioelectron.*, 2019, **126**, 36–43.
71 M. N. Sonuç Karaboğa and M. K. Sezgintürk, *J. Pharm. Biomed. Anal.*, 2018, **154**, 227–235.
72 N. Alshehri, S. Eissa, L. Balobaid, A. M. Abdel Rahman, M. Dasouki and M. Zourob, *Electroanalysis*, 2017, **29**, 1911–1917.
73 B. Demirbakan and M. K. Sezgintürk, *Talanta*, 2017, **169**, 163–169.
74 B. Özcan and M. K. Sezgintürk, *J. Electroanal. Chem.*, 2017, **792**, 31–38.
75 B. Özcan and M. K. Sezgintürk, *Talanta*, 2016, **160**, 367–374.
76 X. Li and X. Liu, *Adv. Healthcare Mater.*, 2016, **5**, 1378.
77 D. Zhang, Y. Lu, Q. Zhang, L. Liu, S. Li, Y. Yao, J. Jiang, G. L. Liu and Q. Liu, *Sens. Actuators, B*, 2016, **222**, 994–1002.
78 J. Cecchetto, F. C. Carvalho, A. Santos, F. C. B. Fernandes and P. R. Bueno, *Sens. Actuators, B*, 2015, **213**, 150–154.
79 S. Singal, A. K. Srivastava, S. Dhakate, A. M. Biradar and Rajesh, *RSC Adv.*, 2015, **5**, 74994–75003.
80 C. C. Mayorga-Martinez, A. Chamorro-Garcia and A. Merkoçi, *Biosens. Bioelectron.*, 2015, **67**, 53–58.
81 U. Jarocka, R. Sawicka, A. Góra-Sochacka, A. Sirko, W. Zagórski-Ostoja, J. Radecki and H. Radecka, *Biosens. Bioelectron.*, 2014, **55**, 301–306.
82 N. S. Ferreira and M. G. F. Sales, *Biosens. Bioelectron.*, 2014, **53**, 193–199.
83 G. Cabral-Miranda, E. H. G. Yamashiro-Kanashiro, M. Gidlund and M. G. F. Sales, *J. Mater. Chem. B*, 2014, **2**, 477–484.
84 Y.-K. Yen, C.-H. Chao and Y.-S. Yeh, *Sensors*, 2020, **20**, 1372.
85 B. Rezaei, H. R. Jamei and A. A. Ensafi, *Biosens. Bioelectron.*, 2018, **115**, 37–44.
86 E. Haghshenas, T. Madrakian, A. Afkhami and H. Saify Nabiabad, *Anal. Bioanal. Chem.*, 2017, **409**, 5269–5278.
87 S. Trashin, M. de Jong, T. Breugelmans, S. Pilehvar and K. De Wael, *Electroanalysis*, 2015, **27**, 32–37.
88 K. Y. P. S. Avelino, G. S. dos Santos, I. A. M. Frías, A. G. Silva-Junior, M. C. Pereira, M. G. R. Pitta, B. C. de Araújo, A. Errachid, M. D. L. Oliveira and C. A. S. Andrade, *J. Pharm. Biomed. Anal.*, 2021, **206**, 114392.
89 A. Asadzadeh-Firouzabadi and H. R. Zare, *Anal. Methods*, 2017, **9**, 3852–3861.
90 A. Benvidi, A. Dehghani Firouzabadi, M. Dehghan Tezerjani, S. M. Moshtaghiun, M. Mazloum-Ardakani and A. Ansarin, *J. Electroanal. Chem.*, 2015, **750**, 57–64.
91 A. Benvidi, N. Rajabzadeh, M. Mazloum-Ardakani, M. M. Heidari and A. Mulchandani, *Biosens. Bioelectron.*, 2014, **58**, 145–152.
92 C. B. A. Hassine, H. Kahri and H. Barhoumi, *J. Iran. Chem. Soc.*, 2022, **19**, 1651–1659.
93 R. Gangwar, C. Subrahmanyam and S. R. K. Vanjari, *ChemistrySelect*, 2021, **6**, 11086–11094.
94 H. Wu, F. Fang, C. Wang, X. Hong, D. Chen and X. Huang, *Biosensors*, 2021, **11**, 216.
95 T. V. Shishkanova, N. Štěpánková, M. Tlustý, T. Tobrman, B. Jurásek, M. Kuchař, M. Trchová, P. Fitl and M. Vrňata, *Electrochim. Acta*, 2021, **373**, 137862.
96 A. Yari and M. Saeidikhah, *Talanta*, 2015, **144**, 1336–1341.
97 S. M. V. Cerqueira, R. Fernandes, F. T. C. Moreira and M. G. F. Sales, *Microchem. J.*, 2021, **164**, 105992.
98 A.-E. Radi, A. Eissa and T. Wahdan, *Int. J. Environ. Anal. Chem.*, 2019, **101**, 2586–2597.
99 A. P. M. Tavares and M. G. F. Sales, *Electrochim. Acta*, 2018, **262**, 214–225.
100 V. Malyshev, A. Michota-Kamińska, S. Shao, F. D'Souza and K. Noworyta, *ECS J. Solid State Sci. Technol.*, 2018, **7**, Q3189–Q3195.
101 L. Han, P. Liu, V. A. Petrenko and A. H. Liu, *Sci. Rep.*, 2016, **6**, 22199.

